

Supporting Information

**Ferrocenyl Naphthalenes: Substituent- and Substitution Pattern-depending
Charge Transfer Studies**

Andrea Preuß,^a Marcus Korb,^b Dominique Miesel,^a Tobias Rüffer,^a Alexander Hildebrandt^a and Heinrich Lang^{a*}

- a) *Technische Universität Chemnitz, Faculty of Natural Sciences, Institute of Chemistry, Inorganic Chemistry, 09107 Chemnitz, Germany*
- b) *Presently, The University of Western Australia, Faculty of Science, School of Molecular Sciences, Crawley, Perth, WA 6009, Australia*

*Corresponding author: Email: heinrich.lang@chemie.tu-chemnitz.de; phone: +49(0)371-531-21210; fax.: +49(0)371-531-21219.

Content:

Table SI1	Crystallographic data for 3a–c and 3e .	pS4
Table SI2	Crystallographic data for 4 and 6b–d .	pS4
Table SI3	Crystallographic data for 7a–d .	pS5
Table SI4	Selected D-Fe bond lengths, angles and torsion angles of 3a–c and 3e	pS6
Table SI5	Selected D-Fe bond lengths, angles and torsion angles of 4 and 6b–d	pS6
Table SI6	Selected D-Fe bond lengths, angles and torsion angles, and plane intersections ($^{\circ}/\text{\AA}$) of 7a–d	pS6
Scheme SI1	Numbering scheme of naphthalene core	pS6
Table SI7	Bond lengths of the naphthalene substituents of 3a–c and 3e	pS7
Table SI8	Bond lengths of the naphthalene substituents of 4 and 6b–d	pS7
Table SI9	Bond lengths of the naphthalene substituents of 7a–d	pS7
Table SI10	Bond lengths of the naphthalene substituents of 7c , 8 and 9	pS8
Table SI11	RMS deviations of the naphthalene planes of 3a–e , 4 , 6b–d and 7a–d	pS8
Figure SI1	ORTEP (50 % probability level) of the molecular structures of 3a and 3b	pS8
Figure SI2	ORTEP (50 % probability level) of the molecular structure of 3e	pS9
Figure SI3	ORTEP (50 % probability level) of the molecular structures of 6b and 6c	pS9
Figure SI4	ORTEP (50 % probability level) of the molecular structure of 6d	pS10
Figure SI5	ORTEP (50 % probability level) of the molecular structure of 7b	pS10
Figure SI6	ORTEP (50 % probability level) of the molecular structure of 7c	pS11
Figure SI7	ORTEP showing the intermolecular <i>T</i> -shaped π -interaction of 3b	pS11
Figure SI8	ORTEP showing the intermolecular <i>T</i> -shaped and parallel displaced π -interactions of 3c	pS12
Figure SI9	ORTEP showing the intermolecular parallel displaced π - π interactions of 3e	pS12
Figure SI10	ORTEP showing the intermolecular <i>T</i> -shaped and parallel displaced π -interaction of 6b	pS13
Figure SI11	ORTEP showing the intermolecular <i>T</i> -shaped π -interaction of 6d	pS13
Figure SI12	ORTEP showing the intermolecular <i>T</i> -shaped π -interactions of 7a	pS14
Figure SI13	ORTEP showing the intramolecular π - π interaction of 7c	pS14
Figure SI14	Cyclic and square wave voltammograms of 3a–e and 4	pS15
Figure SI15	Cyclic and square wave voltammograms of 6a–d	pS15
Scheme SI2	Resonance structures of $[\mathbf{6a}]^+$, $[\mathbf{6b}]^+$, $[\mathbf{6c}]^+$ and $[\mathbf{6d}]^+$	pS16
Figure SI16	Cyclic and square wave voltammogram of 7c in $[\text{N}^n\text{Bu}_4][\text{PF}_6]$	pS16
Figure SI17	vis/NIR spectra and deconvolution of 3a	pS16
Figure SI18	UV/vis/NIR spectra of 3a	pS17
Figure SI19	vis/NIR spectra and deconvolution of 3b	pS17
Figure SI20	UV/vis/NIR spectra of 3b	pS17
Figure SI21	Deconvolution of the NIR spectra of $[\mathbf{3c}]^+$	pS18
Figure SI22	UV/vis/NIR spectra of 3c	pS18
Figure SI23	vis/NIR spectra and deconvolution of 3d	pS18

Figure SI24	UV/vis/NIR spectra of 3d	pS19
Figure SI25	vis/NIR spectra and deconvolution of 3e	pS19
Figure SI26	UV/vis/NIR spectra of 3e	pS19
Figure SI27	vis/NIR spectra and deconvolution of 4	pS20
Figure SI28	UV/vis/NIR spectra of 4	pS20
Figure SI29	vis/NIR spectra and deconvolution of 6a	pS20
Figure SI30	UV/vis/NIR spectra of 6a	pS21
Figure SI31	vis/NIR spectra and deconvolution of 6b	pS21
Figure SI32	UV/vis/NIR spectra of 6b	pS21
Figure SI33	vis/NIR spectra and deconvolution of 6c	pS22
Figure SI34	UV/vis/NIR spectra of 6c	pS22
Figure SI35	Deconvolution of the NIR spectra of [6d]⁺	pS22
Figure SI36	UV/vis/NIR spectra of 6d	pS23
Figure SI37	vis/NIR spectra and deconvolution of 7b	pS23
Figure SI38	UV/vis/NIR spectra of 7b	pS24
Figure SI39	vis/NIR spectra and deconvolution of 7c	pS24
Figure SI40	UV/vis/NIR spectra of 7c	pS25
Figure SI41	UV/vis/NIR spectra of 7d	pS25
Figure SI42	¹ H NMR spectrum of 3a in CDCl ₃	pS26
Figure SI43	¹³ C NMR spectrum of 3a in CDCl ₃	pS26
Figure SI44	¹ H NMR spectrum of 3b in CDCl ₃	pS27
Figure SI45	¹³ C NMR spectrum of 3b in CDCl ₃	pS27
Figure SI46	¹ H NMR spectrum of 3c in CDCl ₃	pS28
Figure SI47	¹³ C NMR spectrum of 3c in CDCl ₃	pS28
Figure SI48	¹ H NMR spectrum of 6a in CDCl ₃	pS29
Figure SI49	¹³ C NMR spectrum of 6a in CDCl ₃	pS29
Figure SI50	¹ H NMR spectrum of 6b in CDCl ₃	pS30
Figure SI51	¹³ C NMR spectrum of 6b in CDCl ₃	pS30
Figure SI52	¹ H NMR spectrum of 6d in CDCl ₃	pS31
Figure SI53	¹³ C NMR spectrum of 6d in CDCl ₃	pS31
Figure SI54	¹ H NMR spectrum of 7a in CDCl ₃	pS32
Figure SI55	¹³ C NMR spectrum of 7a in CDCl ₃	pS32
Figure SI56	¹ H NMR spectrum of 7d in CDCl ₃	pS33
Figure SI57	¹³ C NMR spectrum of 7d in CDCl ₃	pS33

Table SI1. Crystallographic data for **3a–c** and **3e**.

Compound	3a	3b	3c	3e
Empiric formula	C ₂₀ H ₁₆ Fe	C ₂₁ H ₁₈ FeO	C ₂₁ H ₁₈ Fe	C ₂₁ H ₁₆ FeO
M _r , g/mol	312.18	342.20	326.20	340.19
λ, Å	0.71073	0.71073	1.54184	1.54184
Crystal system	orthorhombic	monoclinic	monoclinic	orthorhombic
Space group	<i>Pbca</i>	<i>P2₁/c</i>	<i>P2₁/c</i>	<i>Pna2₁</i>
a, Å	20.2076(13)	15.3517(15)	9.662(5)	8.707(10)
b, Å	6.0150(4)	7.3645(7)	10.031(5)	9.473(3)
c, Å	22.725(2)	14.7940(14)	15.390(5)	36.37(3)
α, deg	90	90	90	90
β, deg	90	115.885(3)	94.773(5)	90
γ, deg	90	90	90	90
V, Å ³	2762.2(4)	1504.8(3)	1486.4(12)	3000.0(5)
ρ _{calcd} mg m ⁻³	1.501	1.511	1.458	1.506
Z	8	4	4	8
μ, mm ⁻¹	1.080	1.004	8.046	8.054
T, K	114.7(4)	100	100	121(1)
Θ range, deg	3.516 – 24.995	3.761 – 25.000	5.217 – 65.987	4.824 – 64.990
Measured reflections	18663	12544	17497	8386
Independent reflections	2411	2638	2589	4410
R _{int}	0.0836	0.0518	0.0360	0.0595
R ₁	0.0367	0.0321	0.0270	0.0720
wR ₂ , (I > 2σ(I))	0.0784	0.0847	0.0682	0.1836
CCDC no.	1897600	1897601	1897602	1897603

Table SI2. Crystallographic data for **4** and **6b–d**.

Compound	4	6b	6c	6d
Empiric formula	C ₃₀ H ₂₂ Fe	C ₂₀ H ₁₅ BrFe	C ₂₀ H ₁₅ BrFe	C ₂₀ H ₁₅ BrFe
M _r , g/mol	438.32	391.08	391.07	391.08
λ, Å	0.71073	0.71073	1.54184	0.71073
Crystal system	monoclinic	monoclinic	monoclinic	orthorhombic
Space group	<i>C2/c</i>	<i>P2₁/c</i>	<i>P2₁/c</i>	<i>Pbca</i>
a, Å	12.8866(8)	12.3825(5)	13.8326(7)	10.3319(10)
b, Å	7.5244(4)	7.7378(4)	11.0072(7)	7.7884(7)
c, Å	21.0448(17)	15.7332(7)	10.0041(5)	37.581(4)
α, deg	90	90	90	90
β, deg	101.335(7)	93.903(3)	96.575(4)	90
γ, deg	90	90	90	90

V , Å ³	2000.8(2)	1503.95(12)	1513.19(14)	3024.1(5)
ρ_{calcd} mg m ⁻³	1.455	1.727	1.717	1.718
Z	4	4	4	8
μ , mm ⁻¹	0.769	3.652	10.999	3.632
T , K	130.00(14)	130.00(10)	119(4)	125(10)
ϑ range, deg	3.151 – 25.495	2.979 – 26.000	5.148 – 62.489	2.930 – 24.998
Measured reflections	6221	10528	4355	8085
Independent reflections	6221	2950	2364	2658
R_{int}	0.0538	0.0268	0.0391	0.0648
R_1	0.0751	0.0236	0.0407	0.0475
wR ₂ , ($I > 2\sigma(I)$)	0.1498	0.0555	0.1050	0.0781
CCDC no.	1897604	1897605	1897606	1897607

Table SI3. Crystallographic data for **7a–d**.

Compound	7a	7b	7c	7d
Empiric formula	C ₃₀ H ₂₄ Fe ₂			
M_r , g/mol	496.19	496.19	496.19	496.19
λ , Å	0.71073	1.54184	0.71073	0.71073
Crystal system	orthorhombic	monoclinic	monoclinic	monoclinic
Space group	<i>Pna</i> 2 ₁	<i>P2</i> ₁ / <i>n</i>	<i>P2</i> ₁ / <i>c</i>	<i>P2</i> ₁ / <i>n</i>
a , Å	12.1550(4)	9.6644(16)	17.0392(7)	13.6264(18)
b , Å	12.9938(3)	10.7292(16)	10.0481(5)	9.7347(13)
c , Å	13.7119(4)	10.9942(18)	12.2011(5)	8.1052(11)
α , deg	90	90	90	90
β , deg	90	110.625(18)	92.020(3)	95.977(4)
γ , deg	90	90	90	90
V , Å ³	2165.65(11)	1066.9(3)	2087.67(16)	1069.3(2)
ρ_{calcd} mg m ⁻³	1.522	1.545	1.579	1.541
Z	4	2	4	2
μ , mm ⁻¹	1.356	11.006	1.406	1.373
T , K	129.95(10)	117(10)	125(10)	100
ϑ range, deg	2.971 – 25.999	5.252 – 64.967	3.342 – 24.997	3.498 – 24.991
Measured reflections	8109	3123	10121	9787
Independent reflections	3646	1782	3653	1869
R_{int}	0.0269	0.0690	0.0225	0.0744
R_1	0.0319	0.0732	0.0259	0.0470
wR ₂ , ($I > 2\sigma(I)$)	0.0689	0.1985	0.0599	0.1081
CCDC no.	1897608	1897609	1897610	1897611

Table SI4. Selected D–Fe bond lengths, angles and torsion angles of **3a–c** and **3e**.

	3a	3b	3c	3e
D1–Fe1 (Å)		1.6459(3)	1.6493(7)	1.646(13)
D2–Fe1 (Å)		1.6489(3)	1.6524(7)	1.645(15)
D3–Fe2 (Å)				1.645(13)
D4–Fe2 (Å)				1.649(15)
D1–Fe1–D2 (°)	179.72(3)	178.16(2)	177.35(2)	177(3)
D3–Fe2–D4 (°)				178(3)
C ₅ H ₄ (D1)–C ₆ (C11) (°)	9.34(12)	46.98(9)	39.97(7)	45.2(5)
C ₅ H ₄ (D3)–C ₆ (C32) (°)				45.2(5)
C1–D1–D2–C6 (°)		−3.87(15)	0.93(11)	−0.2(8)
C1–D1–D2–C10 (°)	5.4 (2)			
C22–D3–D4–C27 (°)				0.6(8)

D1 = centroid of C1–C5; D2 = centroid of C6–C10.

Table SI5. Selected D–Fe bond lengths, angles and torsion angles of **4** and **6b–d**.

	4	6b	6c	6d
D1–Fe1 (Å)	1.6576(1)	1.6452(3)	1.6595(6)	1.6480(6)
D2–Fe1 (Å)		1.6450(3)	1.6550(6)	1.6510(5)
D1–Fe1–D2 (°)		177.30(2)	177.48(4)	179.53(5)
C ₅ H ₄ (D1)–C ₆ (C11) (°)		39.06(7)	58.26(16)	14.9(2)
C ₅ H ₄ (D1)–C ₆ (C6) (°)	77.59(19)			
C1–D1–D2–C6 (°)		2.91(14)	−10.3(3)	−11.3(3)

D1 = centroid of C1–C5; D2 = centroid of C6–C10; D3 = centroid of C22–C26; D4 = centroid of C27–C31.

Table SI6. Selected D–Fe bond lengths, angles and torsion angles, and plane intersections (°/Å) of **7a–d**.

	7a	7b	7c	7d
D1–Fe1 (Å)	1.643(6)	1.6433(8)	1.6537(3)	1.6434(5)
D2–Fe1 (Å)	1.644(8)	1.6469(8)	1.6507(3)	1.6457(5)
D3–Fe2 (Å)	1.644(9)		1.6521(3)	
D4–Fe2 (Å)	1.650(8)		1.6512(3)	
D1–Fe1–D2 (°)	173.2(10)	179.26(6)	178.70(2)	178.64(4)
D3–Fe2–D4 (°)	176.6(10)		178.82(2)	
C ₅ H ₄ (D1)–C ₆ (C11) (°)		46.6(3)	40.02(7)	6.1(2)
C ₅ H ₄ (D1)–C ₆ (C21) (°)	52.57(15)		37.42(7)	
C ₅ H ₄ (D3)–C ₆ (C24) (°)	41.62(18)			
C1–D1–D2–C6 (°)	−19(10)	6.6(4)	−15.22(13)	2.2(3)
C11–D3–D4–C16 (°)	3.9(3)		3.15(12)	
C ₅ H ₄ ^A ...C ₅ H ₄ ^B	180.0(4)	151.37(6)	88.82(17)	180.0(3)

D1 = centroid of C1–C5; D2 = centroid of C6–C10; D3 = centroid of C11–C15; D4 = centroid of C16–C20.

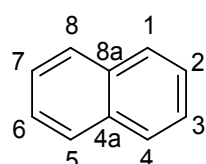
A, B = planes of cyclopentadienyls, according to an ascending labeling. The plane intersection is given while considering the orientation of the attached Fe(C₅H₅) fragment.**Scheme SI1.** Numbering scheme of naphthalene core.

Table SI7. Bond lengths of the naphthalene substituents of **3a–c** and **3e**.

	3a	3b	3c	3e (1)	3e (2)
C1–C2 (Å)	1.374(4)	1.387(3)	1.391(3)	1.397(18)	1.396(17)
C2–C3 (Å)	1.418(3)	1.409(3)	1.422(3)	1.42(2)	1.411(18)
C3–C4 (Å)	1.356(4)	1.361(3)	1.355(3)	1.34(2)	1.351(19)
C4–C4a (Å)	1.417(4)	1.408(3)	1.412(3)	1.427(19)	1.422(18)
C4a–C5 (Å)	1.414(4)	1.417(3)	1.413(3)	1.397(19)	1.422(19)
C4a–C8a (Å)	1.420(4)	1.427(3)	1.430(2)	1.430(19)	1.433(18)
C5–C6 (Å)	1.360(4)	1.364(3)	1.365(3)	1.381(19)	1.36(2)
C6–C7 (Å)	1.409(4)	1.404(3)	1.409(3)	1.41(2)	1.40(2)
C7–C8 (Å)	1.361(4)	1.369(3)	1.377(3)	1.36(2)	1.380(19)
C8–C8a (Å)	1.412(4)	1.419(3)	1.417(3)	1.430(18)	1.424(17)
C8a–C1 (Å)	1.419(4)	1.430(3)	1.448(3)	1.430(18)	1.431(18)

(1) = the first molecule in the asymmetric unit of **3e**; (2) = the second molecule in the asymmetric unit of **3e**.**Table SI8.** Bond lengths of the naphthalene substituents of **4** and **6b–d**.

	4	6b	6c	6d
C1–C2 (Å)	1.369(8)	1.374(3)	1.379(6)	1.381(5)
C2–C3 (Å)	1.408(8)	1.411(3)	1.421(6)	1.426(5)
C3–C4 (Å)	1.355(8)	1.357(3)	1.342(6)	1.361(6)
C4–C4a (Å)	1.414(8)	1.419(3)	1.412(7)	1.415(6)
C4a–C5 (Å)	1.420(8)	1.418(3)	1.423(7)	1.418(6)
C4a–C8a (Å)	1.432(8)	1.433(3)	1.441(6)	1.427(5)
C5–C6 (Å)	1.352(9)	1.359(3)	1.349(8)	1.365(6)
C6–C7 (Å)	1.414(8)	1.416(3)	1.400(7)	1.404(5)
C7–C8 (Å)	1.369(8)	1.356(3)	1.384(7)	1.363(6)
C8–C8a (Å)	1.401(8)	1.422(3)	1.425(6)	1.409(6)
C8a–C1 (Å)	1.440(8)	1.429(3)	1.433(6)	1.411(6)

Table SI9. Bond lengths of the naphthalene substituents of **7a–d**.

	7a	7b	7c	7d
C1–C2 (Å)	1.369(5)	1.377(8)	1.376(3)	1.385(5)
C2–C3 (Å)	1.395(6)	1.414(8)	1.402(3)	1.411(5)
C3–C4 (Å)	1.373(6)	1.356(9)	1.355(3)	1.362(5)
C4–C4a (Å)	1.447(5)		1.410(3)	
C4a–C5 (Å)	1.419(6)		1.412(3)	
C4a–C8a (Å)	1.420(6)		1.434(3)	
C5–C6 (Å)	1.361(5)		1.363(3)	
C6–C7 (Å)	1.393(6)		1.402(3)	
C7–C8 (Å)	1.361(6)		1.374(3)	
C8–C8a (Å)	1.418(5)		1.437(3)	
C8a–C1 (Å)	1.437(5)	1.422(8)	1.435(2)	1.417(5)

Table SI10. Bond lengths of the naphthalenes substituent of **7c**^[1], 1,8-Bis(cobaltocenyl)naphthalene^[2] (**8**) and 1,8-Bis[(η⁵-pentamethylcyclopentadienyl)(η⁵-cyclopentadienyl)-nickel(II)]naphthalene^[3] (**9**).

	7c ^[1]	8 ^[2]	9 ^[3]
C1–C2 (Å)	1.380	1.389	1.382
C2–C3 (Å)	1.406	1.409	1.407
C3–C4 (Å)	1.341	1.368	1.357
C4–C4a (Å)	1.422	1.419	1.420
C4a–C5 (Å)	1.411	1.422	1.420
C4a–C8a (Å)	1.429	1.431	1.427
C5–C6 (Å)	1.353	1.367	1.360
C6–C7 (Å)	1.394	1.411	1.399
C7–C8 (Å)	1.380	1.390	1.379
C8–C8a (Å)	1.437	1.446	1.443
C8a–C1 (Å)	1.443	1.443	1.444

Table SI11. RMS (root mean square) deviations of the naphthalene planes of compounds **3a–e**, **6b–d** and **7a–d** and the atom showing the highest displacement (d_{max} / Å).*

Compd.	RMS	d _{max}	Compd.	RMS	d _{max}
3a	0.0185	0.034(2) C11	6c	0.0893	0.150(3) C11
3b	0.0466	0.0861(16) C11	C _{11–14}	0.0160	Angle: 10.9(4)°
C _{11–14}	0.0137	Angle: 7.23(19)°	C _{16–19}	0.0169	0.320(7) Br1 ^{a)}
C _{16–19}	0.0078		6d	0.0242	0.037(3) C2
3c	0.0138	0.0257(14) C14	7a	0.0156	0.026(3) C23
3e	0.0321	0.065(10) C11	7b	0.0182	0.020(4) C11
	0.0290	0.067(10) C32	7c	0.1136	0.1894(14) C1
4	0.0125	0.021(5) C6	C _{1–4}	0.0163	Angle: 15.54(14)
6b	0.0247	0.0349(18) C18	C _{6–9}	0.0191	0.007(3) C14
			7d	0.0350	

* The values were calculated by using WinGX. ^{a)} Deviation towards the C16–C19 plane.

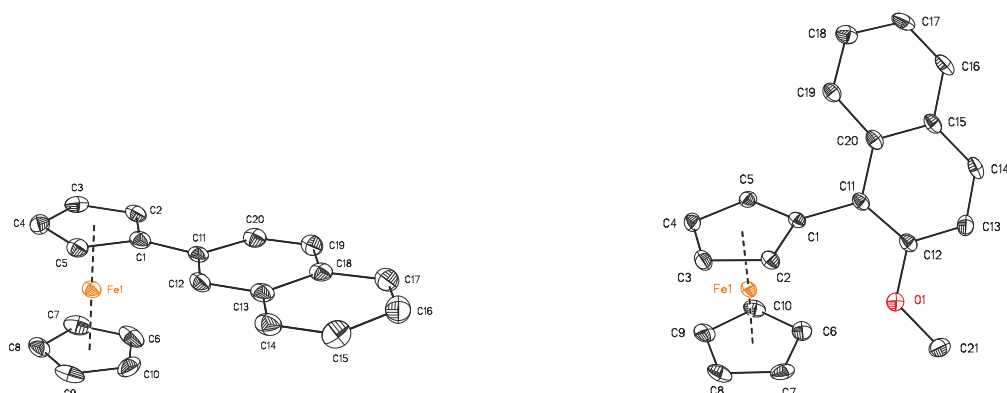


Figure SI1. ORTEP (50 % probability level) of the molecular structures of **3a** (left) and **3b** (right) with the atom-numbering scheme. All hydrogen atoms have been omitted for clarity. Selected bond distances (Å), angles (deg), and torsion angles (deg): **3a**, C1–C11 = 1.471(4), C2–C1–C11 = 126.6(2), C5–C1–C11 = 126.6(2), C11–C1–C2–C3 = -175.1(2), C11–C1–C5–C4 = 174.9(2), C2–C1–C11–C12 = 178.0(2), C5–C1–C11–C12 = 2.9(4), C1–C11–C12–C13 = -173.7(2), C5–C1–C11–C20 = -173.0(2), C2–C1–C11–C20 = 2.1(4); **3b**, C1–C11 = 1.477(3), C12–O1 = 1.367(3), C21–O1 = 1.426(3), C2–C1–C11 = 128.02(19), C5–C1–C11 = 125.43(19), C12–O1–C21 = 118.33(17), C11–C1–C2–C3 = 174.39(19), C11–C1–C5–C4 = -174.71(19), C2–C1–C11–C12 = 48.7(3), C5–C1–C11–C12 = -135.9(2), C1–C11–C12–C13 = 172.24(19), C5–C1–C11–C20 = 45.5(3), C2–C1–C11–C20 = -129.9(2), C11–C12–O1–C21 = -10.2(3).

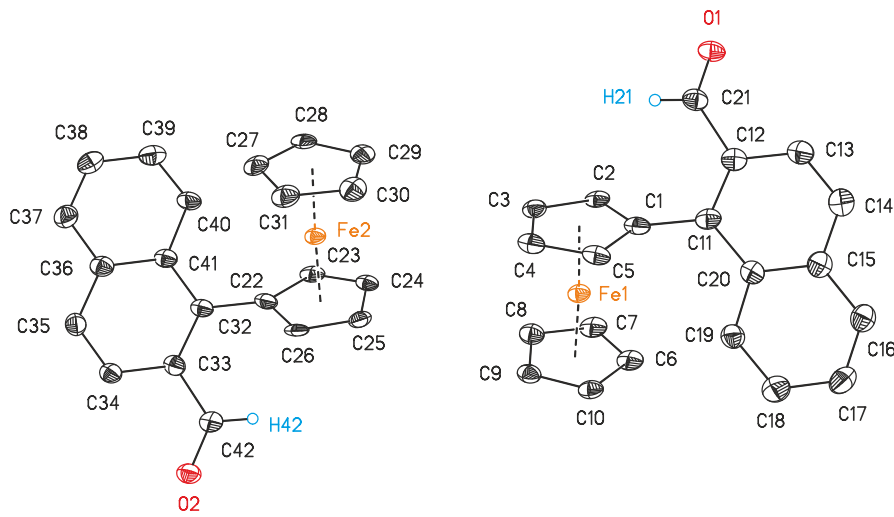


Figure SI2. ORTEP (50 % probability level) of the molecular structure of **3e** with the atom-numbering scheme. All hydrogen atoms have been omitted for clarity. Selected bond distances (\AA), angles (deg), and torsion angles (deg): C1–C11 = 1.480(18), C22–C32 = 1.458(18), C21–O1 = 1.214(16), C21–H21 = 0.9300, C42–O2 = 1.234(15), C42–H42 = 0.9300, C5–C1–C11 = 129.2(12), C2–C1–C11 = 123.5(11), O1–C21–C12 = 124.7(13), O1–C21–H21 = 117.7, C12–C21–H21 = 117.7, C23–C22–C32 = 131.1(12), C26–C22–C32 = 123.2(11), O2–C42–C33 = 123.4(11), O2–C42–H42 = 118.3, C33–C42–H42 = 118.3, C11–C1–C2–C3 = -174.3(11), C11–C1–C5–C4 = 173.9(12), C2–C1–C11–C12 = 40.9(18), C5–C1–C11–C12 = -133.9(13), C1–C11–C12–C13 = -170.7(12), C5–C1–C11–C20 = 50.4(19), C2–C1–C11–C20 = -134.8(13), C32–C22–C23–C24 = -175.8(12), C32–C22–C26–C25 = 174.8(11), C23–C22–C32–C33 = 131.6(13), C26–C22–C32–C33 = -41.6(17), C22–C32–C33–C34 = 170.6(11), C26–C22–C32–C41 = 135.7(12), C23–C22–C32–C41 = -51.1(19), C11–C12–C21–O1 = -168.1(12), C13–C12–C21–O1 = 17.6(19), C32–C33–C42–O2 = 168.9(12), C34–C33–C42–O2 = -15.1(18).

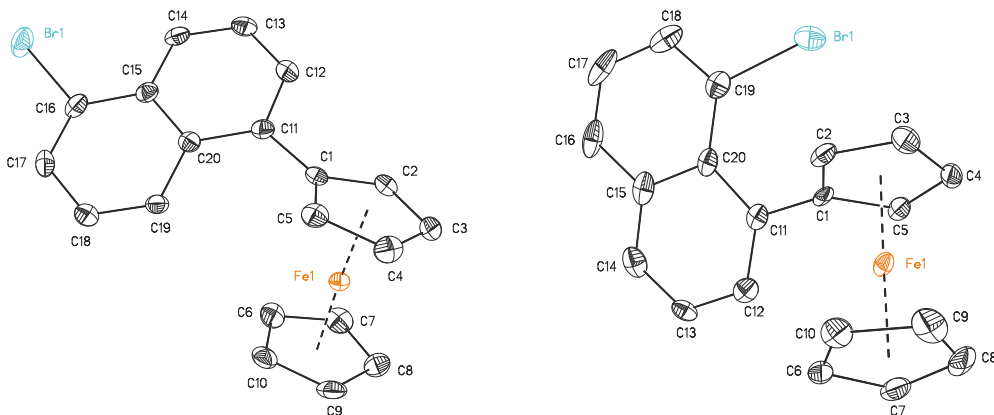


Figure SI3. ORTEP (50 % probability level) of the molecular structures of **6b** (left) and **6c** (right) with the atom-numbering scheme. All hydrogen atoms have been omitted for clarity. Selected bond distances (\AA), angles (deg), and torsion angles (deg): **6b**, C1–C11 = 1.488(3), C16–Br1 = 1.911(2), C2–C1–C11 = 124.02(18), C5–C1–C11 = 129.04(18), C17–C16–Br1 = 117.84(16), C15–C16–Br1 = 118.71(15), C11–C1–C2–C3 = 172.64(18), C11–C1–C5–C4 = -172.22(19), C2–C1–C11–C12 = -34.8(3), C5–C1–C11–C12 = 136.6(2), C1–C11–C12–C13 = -178.1(2), C5–C1–C11–C20 = -40.8(3), C2–C1–C11–C20 = 147.8(2), C14–C15–C16–Br1 = -4.3(3), C20–C15–C16–Br1 = 177.33(14), Br1–C16–C17–C18 = -178.85(16); **6c**, C1–C11 = 1.490(5), C19–Br1 = 1.908(4), C2–C1–C11 = 126.1(3), C5–C1–C11 = 126.1(3), C18–C19–Br1 = 113.8(3), C20–C19–Br1 = 122.9(3), C11–C1–C2–C3 = -176.6(4), C11–C1–C5–C4 = 177.0(4), C2–C1–C11–C12 = -120.5(4), C5–C1–C11–C12 = 62.3(5), C1–C11–C12–C13 = 173.2(3), C5–C1–C11–C20 = -119.8(4), C2–C1–C11–C20 = 57.4(5), C17–C18–C19–Br1 = 171.3(3), Br1–C19–C20–C15 = -163.8(3), Br1–C19–C20–C11 = 13.6(6).

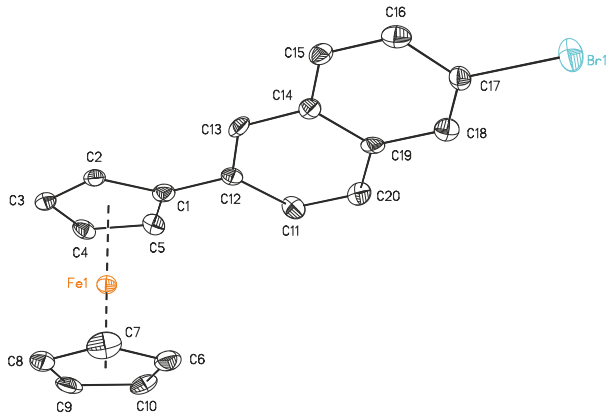


Figure SI4. ORTEP (50 % probability level) of the molecular structure of **6d** with the atom-numbering scheme. All hydrogen atoms have been omitted for clarity. Selected bond distances (\AA), angles (deg), and torsion angles (deg): **6d**, C1–C12 = 1.469(6), C17–Br1 = 1.902(4), C2–C1–C11 = 125.9(4), C5–C1–C11 = 127.1(4), C18–C17–Br1 = 118.6(3), C16–C17–Br1 = 119.1(3), C12–C1–C2–C3 = 179.9(4), C12–C1–C5–C4 = 179.9(4), C11–C12–C1–C2 = -15.1(6), C11–C12–C1–C5 = 164.9(4), C13–C12–C1–C5 = -14.7(6), C13–C12–C1–C2 = 165.4(4), C20–C11–C12–C1 = 178.7(4), C1–C11–C12–C13 = -178.1(2), C15–C16–C17–Br1 = 179.0(3), Br1–C17–C18–C19 = -179.5(3).

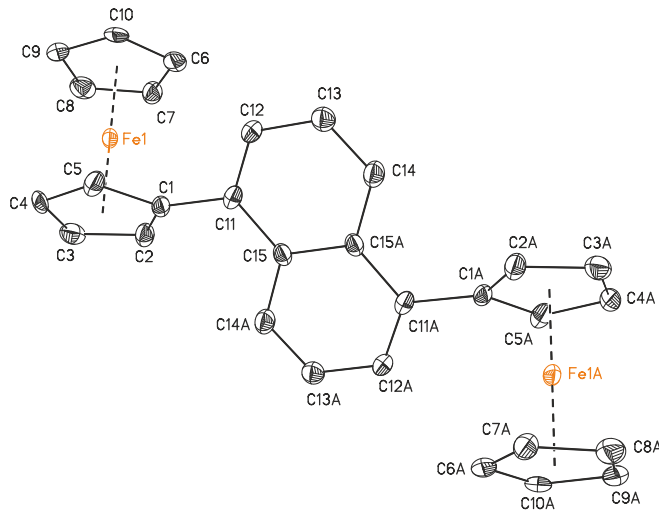


Figure SI5. ORTEP (50 % probability level) of the molecular structure of **7b** with the atom-numbering scheme. All hydrogen atoms have been omitted for clarity. Selected bond distances (\AA) and angles (°): C1–C11 = 1.495(8), C2–C1–C11 = 128.6(5), C5–C1–C11 = 123.8(5), C12–C11–C1 = 119.3(5), C15–C11–C1 = 120.9(5), C11–C1–C2–C3 = 178.7(6), C11–C1–C5–C4 = -179.3(5), C2–C1–C11–C12 = 133.5(6), C5–C1–C11–C12 = -45.7(8), C1–C11–C12–C13 = 179.4(3), C5–C1–C11–C15 = 132.7(6), C2–C1–C11–C15 = -48.1(8). (Symmetry generated atoms are indicated by the suffix A; symmetry code: -x, -y, -z+1.).

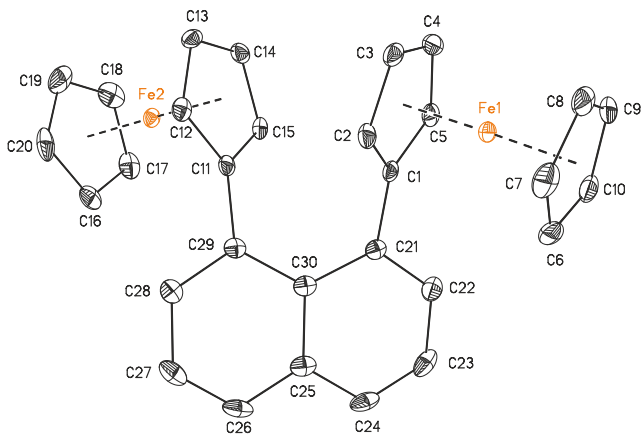
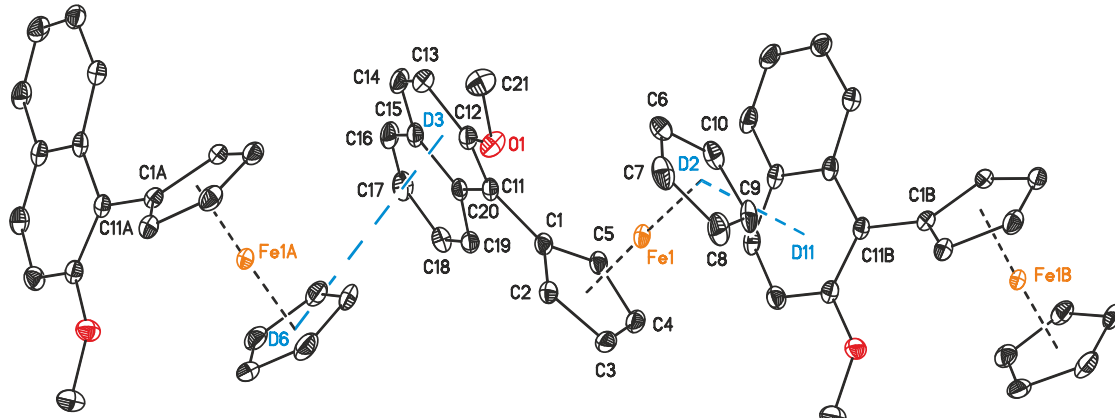


Figure SI6. ORTEP (50 % probability level) of the molecular structure of **7c** with the atom-numbering scheme. All hydrogen atoms have been omitted for clarity. Selected bond distances (Å) and angles (°): C1–C21 = 1.483(3), C11–C29 = 1.481(3), C2–C1–C21 = 126.49(16), C5–C1–C21 = 126.69(16), C30–C21–C1 = 121.86(16), C22–C21–C1 = 119.02(16), C15–C11–C29 = 127.51(16), C12–C11–C29 = 125.46(16), C28–C29–C11 = 119.18(17), C30–C29–C11 = 121.68(16), C21–C1–C2–C3 = –179.72(17), C21–C1–C5–C4 = 179.59(17), C2–C1–C21–C22 = –132.96(19), C5–C1–C21–C22 = 45.7(3), C1–C21–C22–C23 = 169.75(17), C5–C1–C21–C30 = –139.50(18), C2–C1–C21–C30 = 41.9(3), C1–C21–C30–C29 = 19.0(3), C(11)–C(29)–C(30)–C(25) = –161.93(16), C(11)–C(29)–C(30)–C(21) = 17.9(3), C(28)–C(29)–C(11)–C(12) = 43.1(3), C(30)–C(29)–C(11)–C(12) = –141.67(18), C(28)–C(29)–C(11)–C(15) = –135.72(19), C(30)–C(29)–C(11)–C(15) = 39.5(3), C(29)–C(11)–C(15)–C(14) = –179.29(16), C(29)–C(11)–C(12)–C(13) = 179.46(17).



Ct ... D	d (Å)	α (°)
	4.721(16)	85.79(12)

Figure SI7. ORTEP (50 % probability level) of the molecular structure of **3b** with selected atom-numbering scheme, showing the intermolecular *T*-shaped π -interaction (blue dashed lines) between the C₅H₅ unit and the C₆H₄ moiety (including C11 to C20). Only a section of different π - π interaction pattern is shown and all hydrogen atoms have been omitted for clarity. (Symmetry code for generating-equivalent atoms; A: x, 3/2–y, –1/2+z; B: x, 3/2–y, 1/2+z).

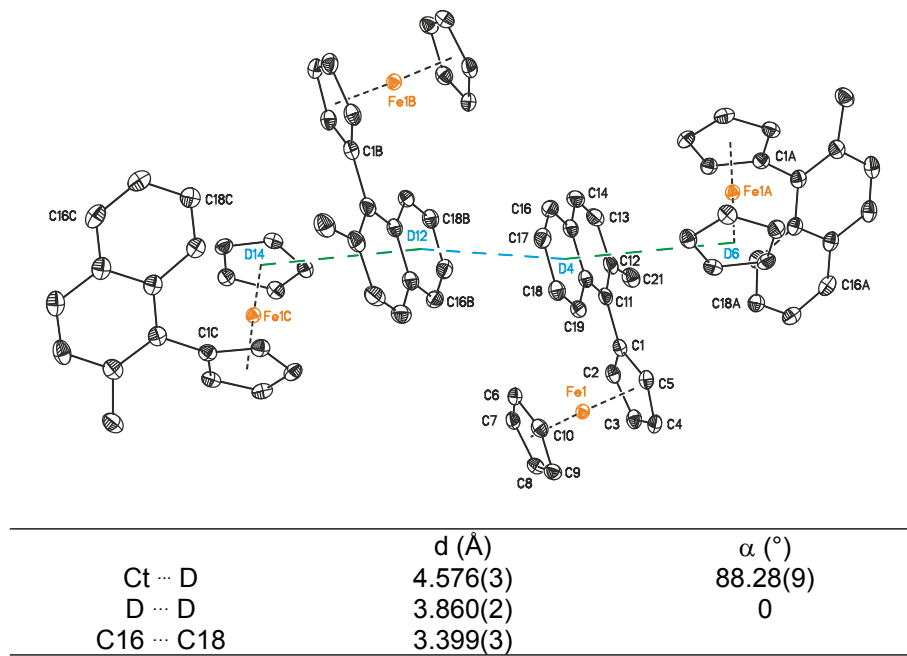


Figure S18. ORTEP (50 % probability level) of the molecular structure of **3c** with selected atom-numbering scheme, showing the intermolecular T -shaped π -interaction (green dashed lines) between the C_5H_5 unit and the C_6H_4 moiety (including C16 and C18) and parallel displaced pattern (blue dashed lines) between the C_6H_4 moieties (including C16 and C18). Only a section of different π - π interaction pattern is shown and all hydrogen atoms have been omitted for clarity. (Symmetry code for generating-equivalent atoms; A: $-1/2+x, 1/2+y, 3/2-z$; B: $-1+x, -y, 1-z$; C: $-1/2+x, 1/2-y, -1/2+z$).

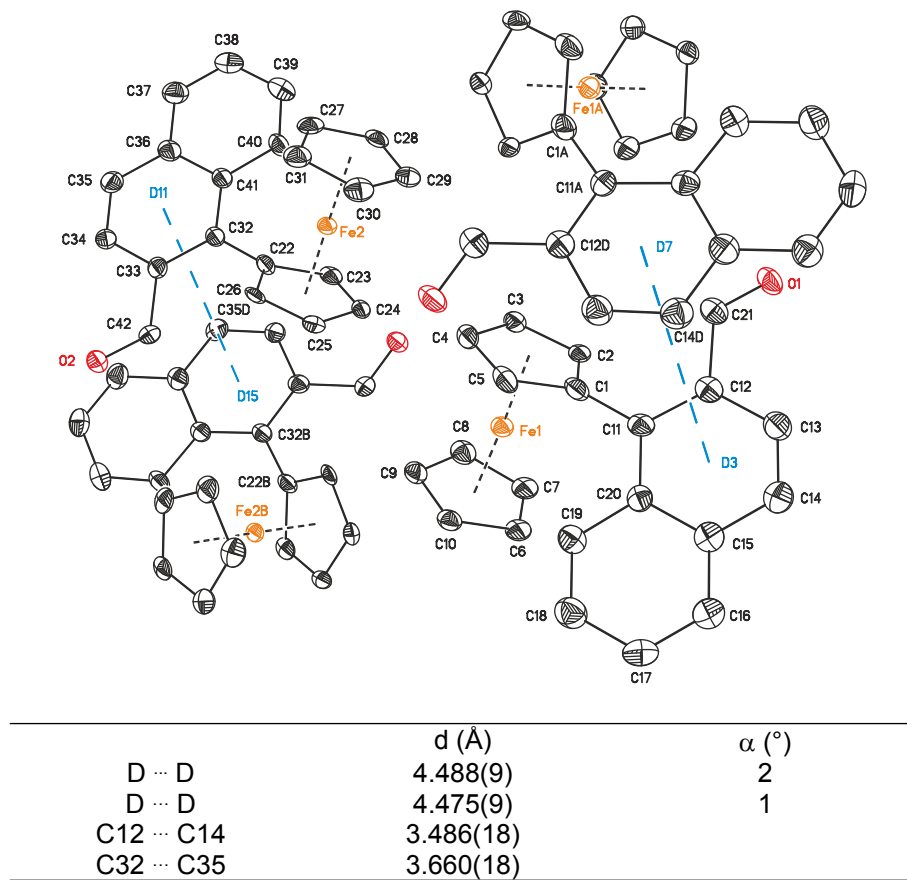
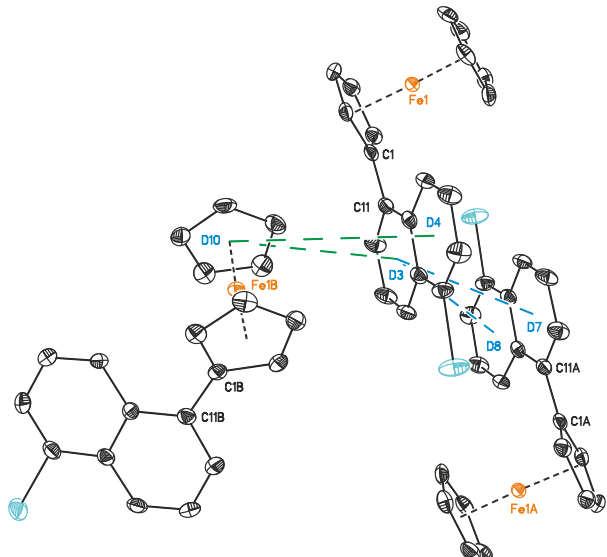


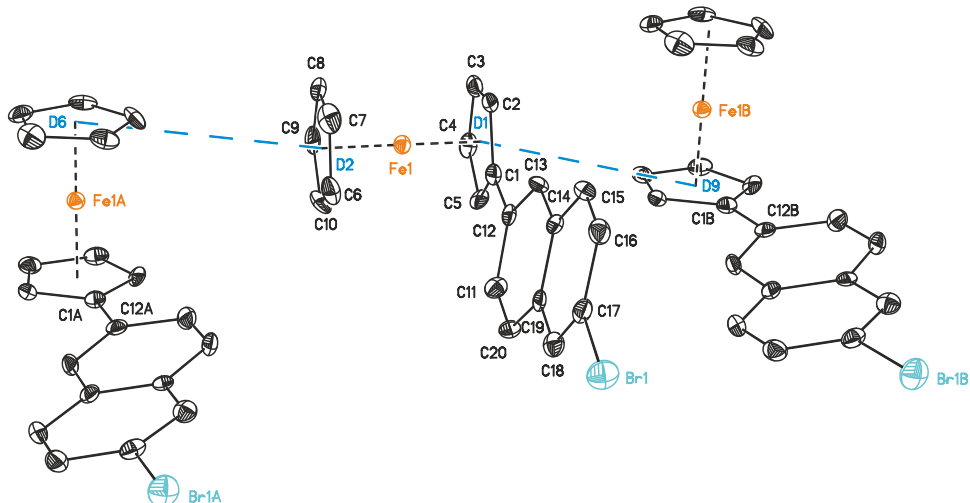
Figure S19. ORTEP (50 % probability level) of the molecular structure of **3e** with selected atom-numbering scheme, showing the intermolecular parallel displaced π -interaction (blue dashed lines)

between the naphthalene moieties (including C11 to C20 and C32 to C41) forming dimers. All hydrogen atoms have been omitted for clarity. (Symmetry code for generating-equivalent atoms; A: $x+1/2$, $3/2-y$, z ; B: $x+1/2$, $3/2-y$, z).



	d (\AA)	α ($^\circ$)
D3 … D10	4.6688(13)	78.12(12)
D4 … D10	4.9217(14)	79.47(12)
D3 … D8	3.8925(13)	0
D3 … D7	4.5528(12)	2.52(10)

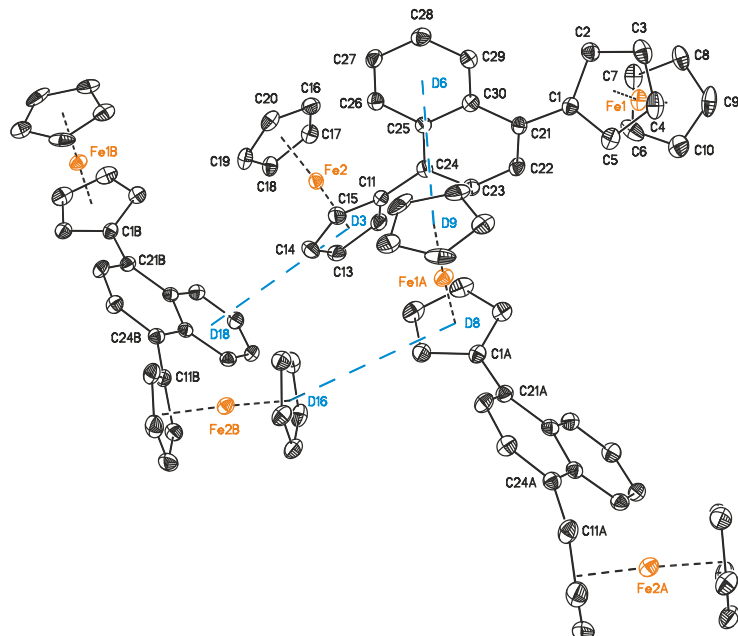
Figure SI10. ORTEP (50 % probability level) of the molecular structure of **6b** with selected atom-numbering scheme, showing the intermolecular T -shaped π -interaction (green dashed lines) between the C_6H_5 unit and the C_6H_4 moiety (including C11 to C20) and parallel displaced pattern (blue dashed lines) between the C_6H_4 moieties (including C11 to C20 and C15 to C20). Only a section of different $\pi-\pi$ interaction pattern is shown and all hydrogen atoms have been omitted for clarity. (Symmetry code for generating-equivalent atoms; A: $2-x$, $1-y$, $2-z$; B: x , $3/2-y$, $1/2-z$).



	d (\AA)	α ($^\circ$)
D2 … D6	4.975(3)	89
D1 … D9	4.648(3)	90

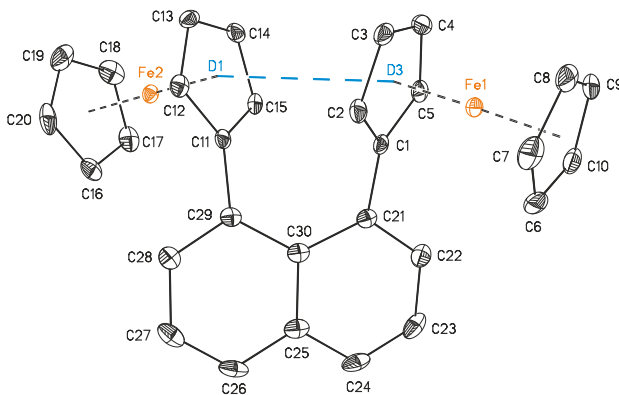
Figure SI11. ORTEP (50 % probability level) of the molecular structure of **6d** with selected atom-numbering scheme, showing the intermolecular T -shaped π -interaction (blue dashed lines) between the

C_5H_5 units and C_4H_5 units. All hydrogen atoms and further interactions have been omitted for clarity. (Symmetry code for generating-equivalent atoms; A: $5/2-x, -1/2+y, z$; B: $5/2-x, 1/2+y, z$).



	d (\AA)	α ($^\circ$)
D8 … D16	4.606(3)	88.7(3)
D9 … D6	4.758(7)	87.5(6)
D3 … D18	4.820(3)	83.7(2)

Figure SI12. ORTEP (50 % probability level) of the molecular structure of **7a** with selected atom-numbering scheme, showing the intermolecular T -shaped π -interaction (blue dashed lines) between the C_5H_5 unit and the C_6H_4 moiety (including C25 to C30). All hydrogen atoms and further interactions have been omitted for clarity. (Symmetry code for generating-equivalent atoms; A: $-x, -y, z-1/2$; B: $1-x, -y, z-1/2$).



	d (\AA)	α ($^\circ$)
D … D	3.860(2)	28.62(11)

Figure SI13. ORTEP (50 % probability level) of the molecular structure of **7c** with selected atom-numbering scheme, showing the intramolecular π - π interaction between the C_5H_5 unit of the ferrocene moieties. All hydrogen atoms have been omitted for clarity.

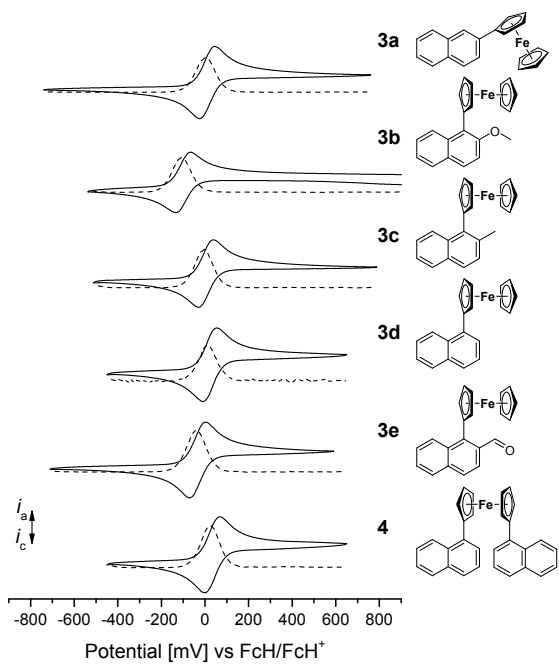


Figure SI14. Cyclic and square wave voltammograms (CV: potential area -1000 to 1000 mV; SW: potential area -1000 to 750 mV) of **3a–3e** and **4**. Conditions: scan rate 100 mV s⁻¹ (CV), 2.5 mV s⁻¹ (SW) in dichloromethane solutions (1.0 mmol L⁻¹), supporting electrolyte 0.1 mol L⁻¹ [$\text{N}^n\text{Bu}_4\text{][B(C}_6\text{F}_5)_4$], working electrode glassy carbon.

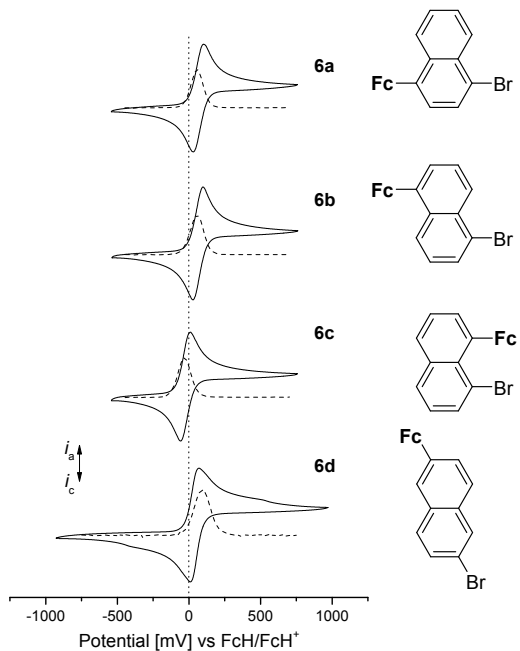
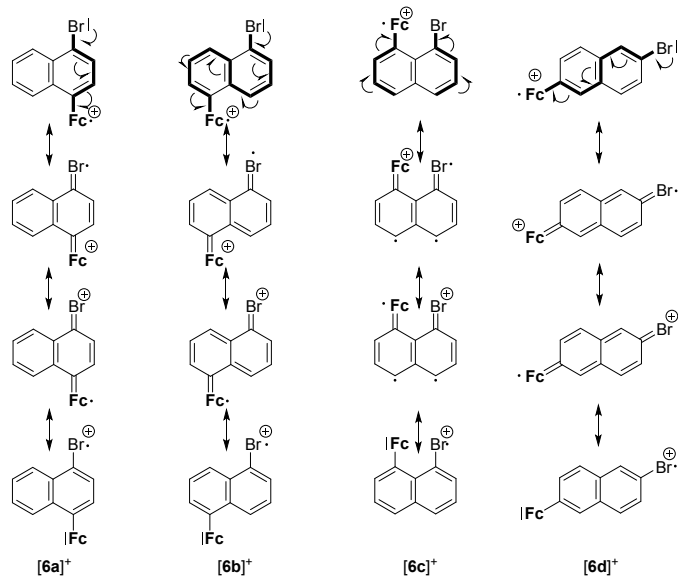


Figure SI15. Cyclic and square wave voltammograms (CV: potential area -1000 to 1000 mV; SW: potential area -1000 to 750 mV) of **6a–d**. Conditions: scan rate 100 mV s⁻¹ (CV), 2.5 mV s⁻¹ (SW) in dichloromethane solutions (1.0 mmol L⁻¹), supporting electrolyte 0.1 mol L⁻¹ [$\text{N}^n\text{Bu}_4\text{][B(C}_6\text{F}_5)_4$], working electrode glassy carbon.



Scheme SI2. Resonance structures illustrating the through-bond charge transfer pathways in $[6\text{a}]^+$, $[6\text{b}]^+$, $[6\text{c}]^+$ and $[6\text{d}]^+$.

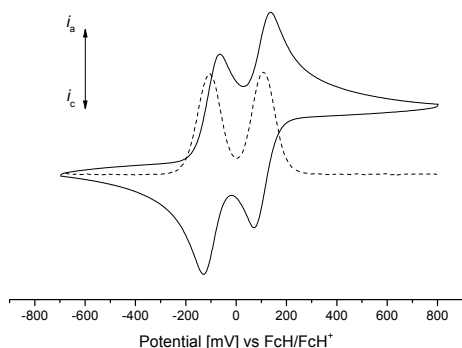


Figure SI16. Cyclic and square wave voltammograms (CV: potential area -500 to 1000 mV; SW: potential area -500 to 750 mV) of **7c**. Conditions: scan rate 100 mV s⁻¹ (CV), 2.5 mV s⁻¹ (SW) in dichloromethane solutions (1.0 mmol L⁻¹), supporting electrolyte 0.1 mol L⁻¹ $[\text{N}^n\text{Bu}_4]\text{[PF}_6]$, working electrode glassy carbon.

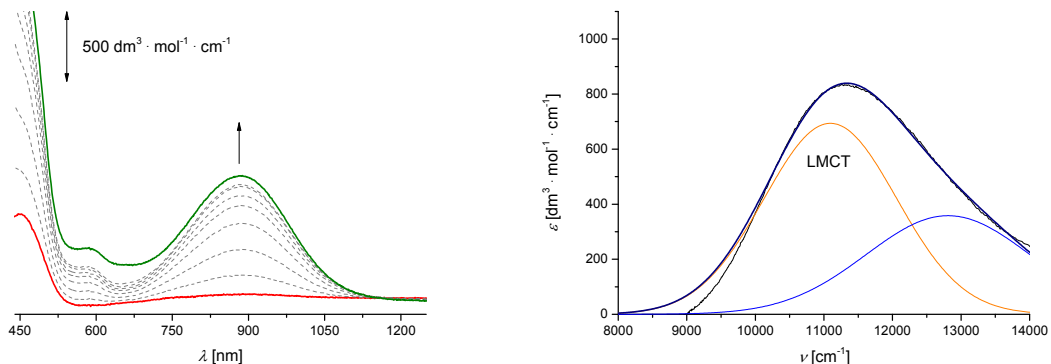


Figure SI17. Left: vis/NIR spectra of **3a** at 25 °C in dichloromethane (2.00 mmol · L⁻¹) at rising potentials (-200 to 1100 mV vs Ag/Ag⁺); supporting electrolyte $[\text{N}^n\text{Bu}_4]\text{[B(C}_6\text{F}_5)_4]$; arrows indicate the increasing absorptions. Right: Deconvolution of the NIR absorption of $[3\text{a}]^+$ using two Gaussian shaped bands.

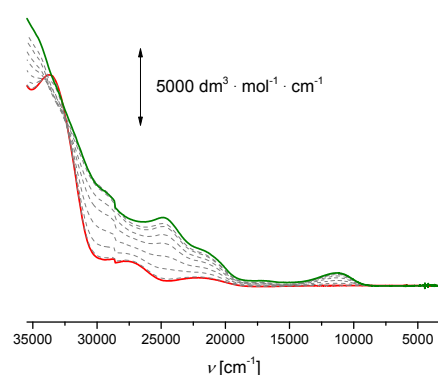


Figure SI18. UV-vis/NIR spectra of **3a** at 25 °C in dichloromethane (2.00 $\text{mmol} \cdot \text{L}^{-1}$) at rising potentials (-200 to 1100 mV vs Ag/Ag⁺); supporting electrolyte [NⁿBu₄][B(C₆F₅)₄].

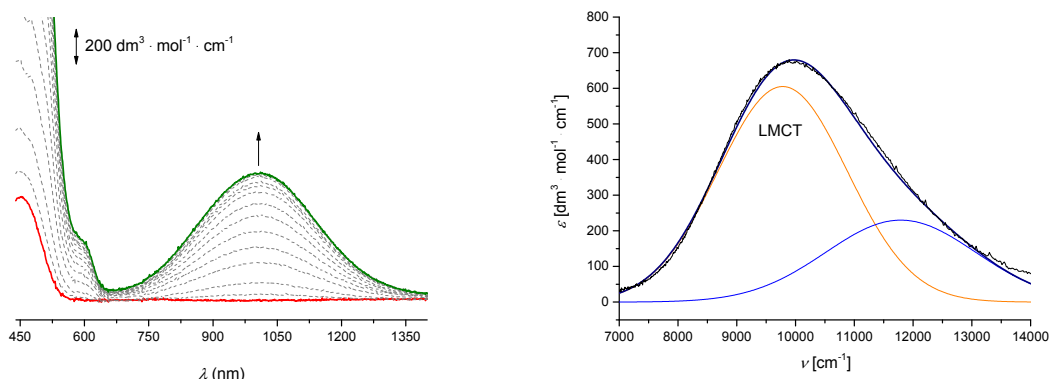


Figure SI19. Left: vis/NIR spectra of **3b** at 25 °C in dichloromethane (2.00 $\text{mmol} \cdot \text{L}^{-1}$) at rising potentials (-200 to 1000 mV vs Ag/Ag⁺); supporting electrolyte [NⁿBu₄][B(C₆F₅)₄]; arrows indicate the increasing absorptions. Right: Deconvolution of the NIR absorption of **[3b]⁺** using two Gaussian shaped bands.

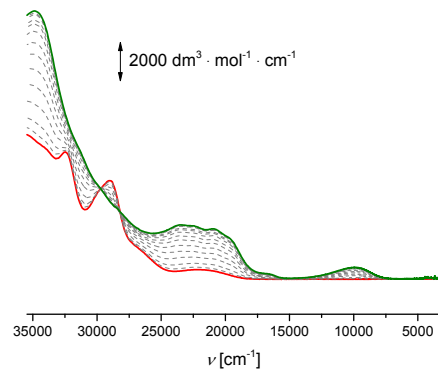


Figure SI20. UV-vis/NIR spectra of **3b** at 25 °C in dichloromethane (2.00 $\text{mmol} \cdot \text{L}^{-1}$) at rising potentials (-200 to 1000 mV vs Ag/Ag⁺); supporting electrolyte [NⁿBu₄][B(C₆F₅)₄].

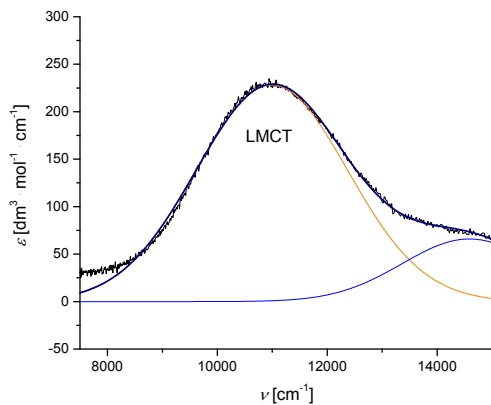


Figure SI21. Deconvolution of the NIR absorption of $[3\mathbf{c}]^+$ using two Gaussian shaped bands.

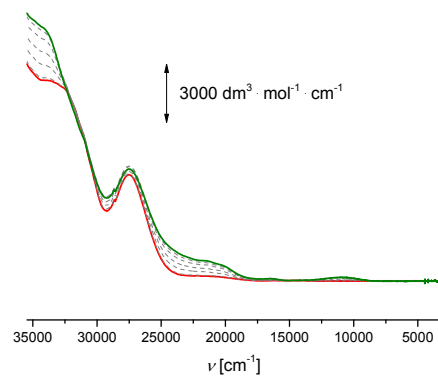


Figure SI22. UV-vis/NIR spectra of $\mathbf{3c}$ at 25 °C in dichloromethane ($2.00 \text{ mmol} \cdot \text{L}^{-1}$) at rising potentials (-200 to 250 mV vs Ag/Ag $^+$); supporting electrolyte $[\text{N}^n\text{Bu}_4][\text{B}(\text{C}_6\text{F}_5)_4]$.

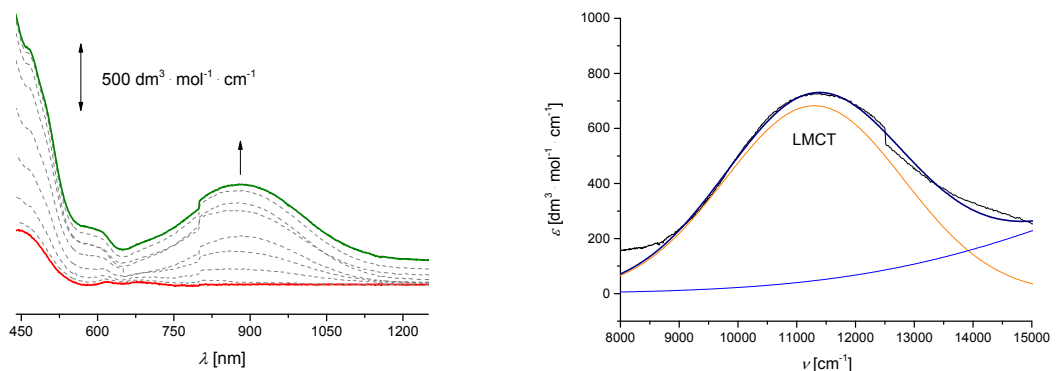


Figure SI23. Left: vis/NIR spectra of $\mathbf{3d}$ at 25 °C in dichloromethane ($2.00 \text{ mmol} \cdot \text{L}^{-1}$) at rising potentials (-200 to 400 mV vs Ag/Ag $^+$); supporting electrolyte $[\text{N}^n\text{Bu}_4][\text{B}(\text{C}_6\text{F}_5)_4]$; arrows indicate the increasing absorptions. Right: Deconvolution of the NIR absorption of $[3\mathbf{d}]^+$ using two Gaussian shaped bands.

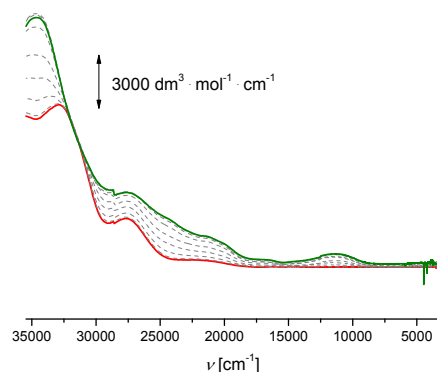


Figure SI24. UV-vis/NIR spectra of **3d** at 25 °C in dichloromethane (2.00 mmol · L⁻¹) at rising potentials (-200 to 400 mV vs Ag/Ag⁺); supporting electrolyte [NⁿBu₄][B(C₆F₅)₄].

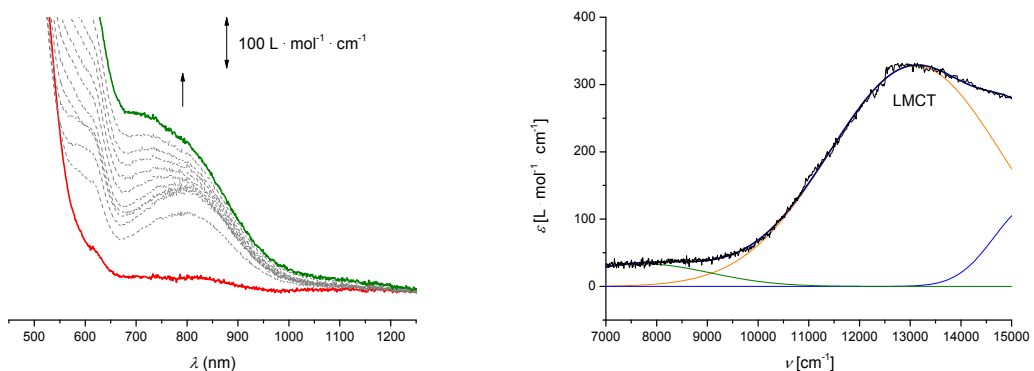


Figure SI25. Left: vis/NIR spectra of **3e** at 25 °C in dichloromethane (2.00 mmol · L⁻¹) at rising potentials (-200 to 950 mV vs Ag/Ag⁺); supporting electrolyte [NⁿBu₄][B(C₆F₅)₄]; arrows indicate the increasing absorptions. Right: Deconvolution of the NIR absorption of **[3e]⁺** using three Gaussian shaped bands.

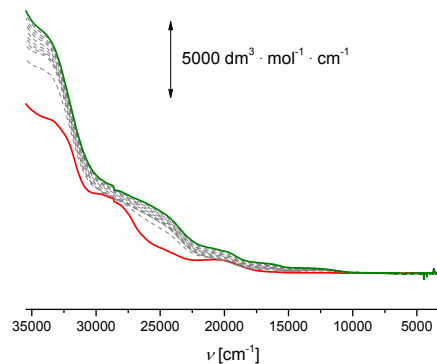


Figure SI26. UV-vis/NIR spectra of **3e** at 25 °C in dichloromethane (2.00 mmol · L⁻¹) at rising potentials (-200 to 950 mV vs Ag/Ag⁺); supporting electrolyte [NⁿBu₄][B(C₆F₅)₄].

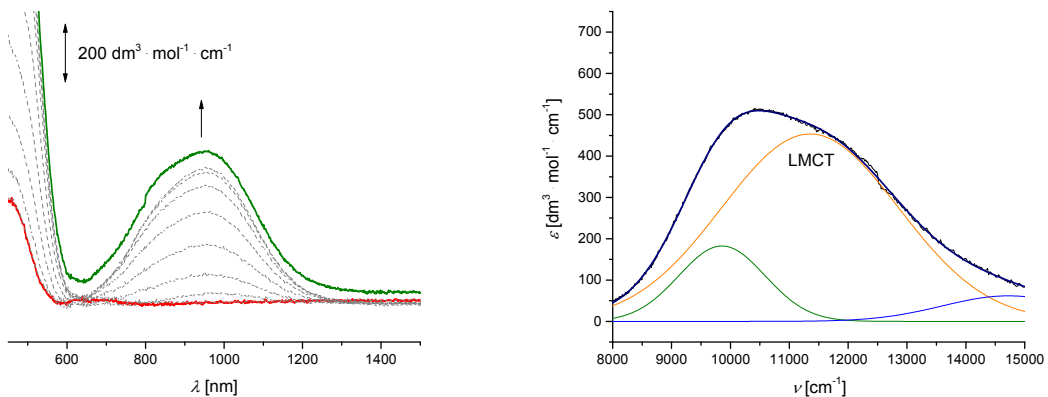


Figure SI27. Left: vis/NIR spectra of **4** at 25 °C in dichloromethane ($2.00 \text{ mmol} \cdot \text{L}^{-1}$) at rising potentials (-200 to 400 mV vs Ag/Ag⁺); supporting electrolyte [$\text{N}^n\text{Bu}_4\text{][B(C}_6\text{F}_5)_4$]; arrows indicate the increasing absorptions. Right: Deconvolution of the NIR absorption of $[\mathbf{4}]^+$ using three Gaussian shaped bands.

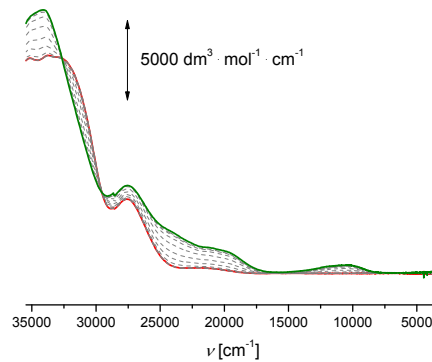


Figure SI28. UV-vis/NIR spectra of **4** at 25 °C in dichloromethane ($2.00 \text{ mmol} \cdot \text{L}^{-1}$) at rising potentials (-200 to 400 mV vs Ag/Ag⁺); supporting electrolyte [$\text{N}^n\text{Bu}_4\text{][B(C}_6\text{F}_5)_4$].

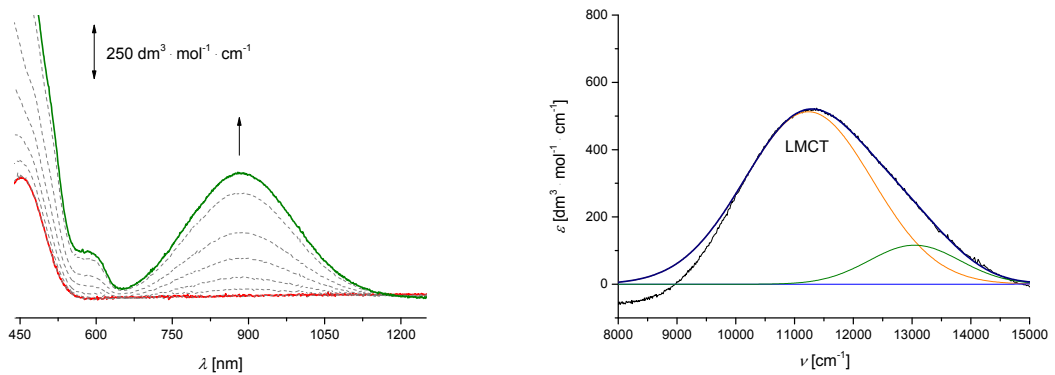


Figure S29. Left: vis/NIR spectra of **6a** at 25 °C in dichloromethane ($2.00 \text{ mmol} \cdot \text{L}^{-1}$) at rising potentials (-200 to 950 mV vs Ag/Ag⁺); supporting electrolyte [$\text{N}^n\text{Bu}_4\text{][B(C}_6\text{F}_5)_4$]; arrows indicate the increasing absorptions. Right: Deconvolution of the NIR absorption of $[\mathbf{6a}]^+$ using three Gaussian shaped bands.

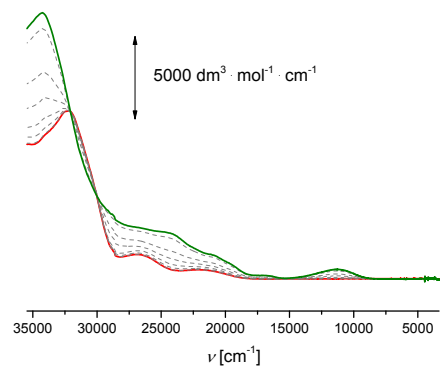


Figure S30. UV-vis/NIR spectra of **6a** at 25 °C in dichloromethane (2.00 mmol · L⁻¹) at rising potentials (-200 to 950 mV vs Ag/Ag⁺); supporting electrolyte [NⁿBu₄][B(C₆F₅)₄].

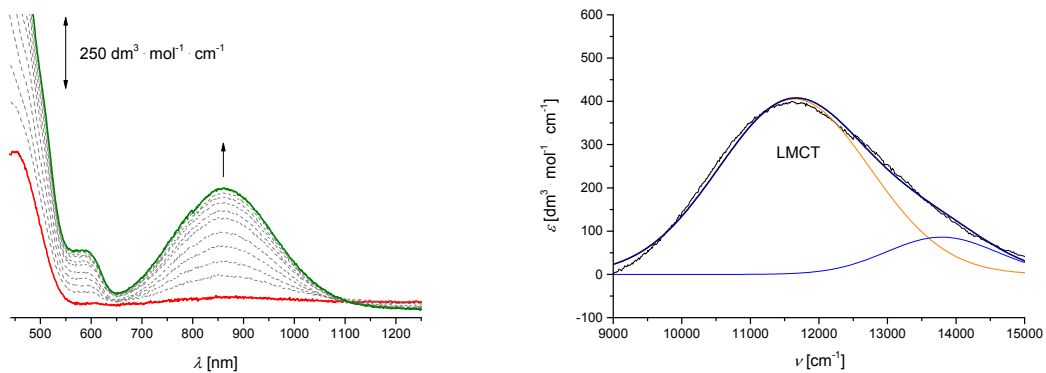


Figure SI31. Left: vis/NIR spectra of **6b** at 25 °C in dichloromethane (2.00 mmol · L⁻¹) at rising potentials (-200 to 1100 mV vs Ag/Ag⁺); supporting electrolyte [NⁿBu₄][B(C₆F₅)₄]; arrows indicate the increasing absorptions. Right: Deconvolution of the NIR absorption of **[6b]⁺** using two Gaussian shaped bands.

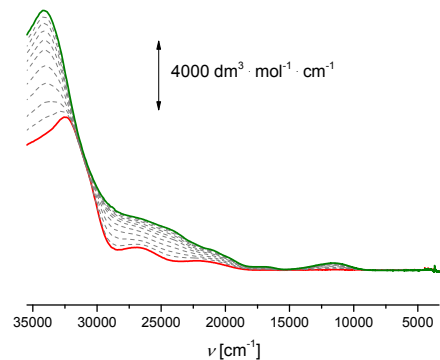


Figure SI32. Left: UV-vis/NIR spectra of **6b** at 25 °C in dichloromethane (2.00 mmol · L⁻¹) at rising potentials (-200 to 1100 mV vs Ag/Ag⁺); supporting electrolyte [NⁿBu₄][B(C₆F₅)₄].

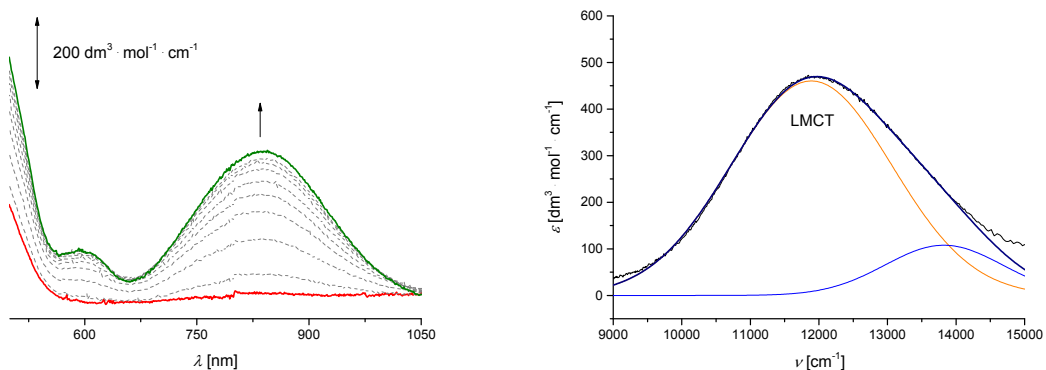


Figure SI33. Left: vis/NIR spectra of **6c** at 25 °C in dichloromethane (2.00 mmol · L⁻¹) at rising potentials (-200 to 800 mV vs Ag/Ag⁺); supporting electrolyte [NⁿBu₄][B(C₆F₅)₄]; arrows indicate the increasing absorptions. Right: Deconvolution of the NIR absorption of **[6c]⁺** using two Gaussian shaped bands.

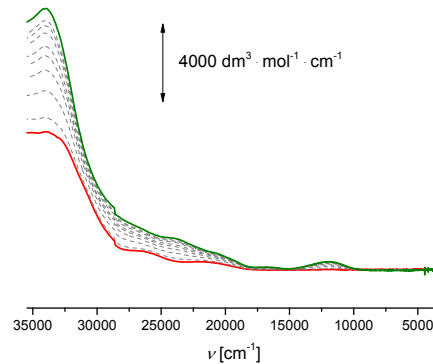


Figure SI34. UV-vis/NIR spectra of **6c** at 25 °C in dichloromethane (2.00 mmol · L⁻¹) at rising potentials (-200 to 800 mV vs Ag/Ag⁺); supporting electrolyte [NⁿBu₄][B(C₆F₅)₄].

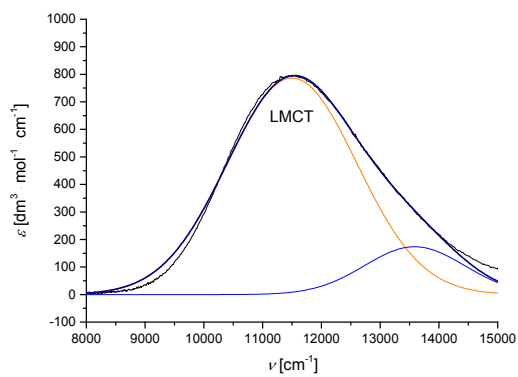


Figure SI35. Deconvolution of the NIR absorption of **[6d]⁺** using two Gaussian shaped bands.

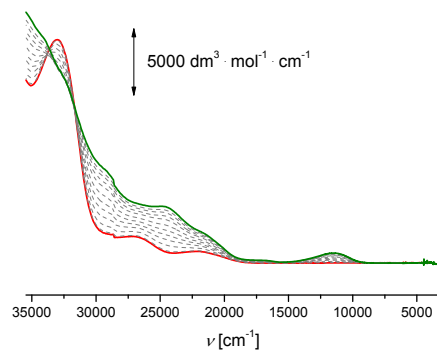


Figure SI36. UV-vis/NIR spectra of **6d** at 25 °C in dichloromethane (2.00 mmol · L⁻¹) at rising potentials (-200 to 900 mV vs Ag/Ag⁺); supporting electrolyte [N⁺Bu₄][B(C₆F₅)₄].

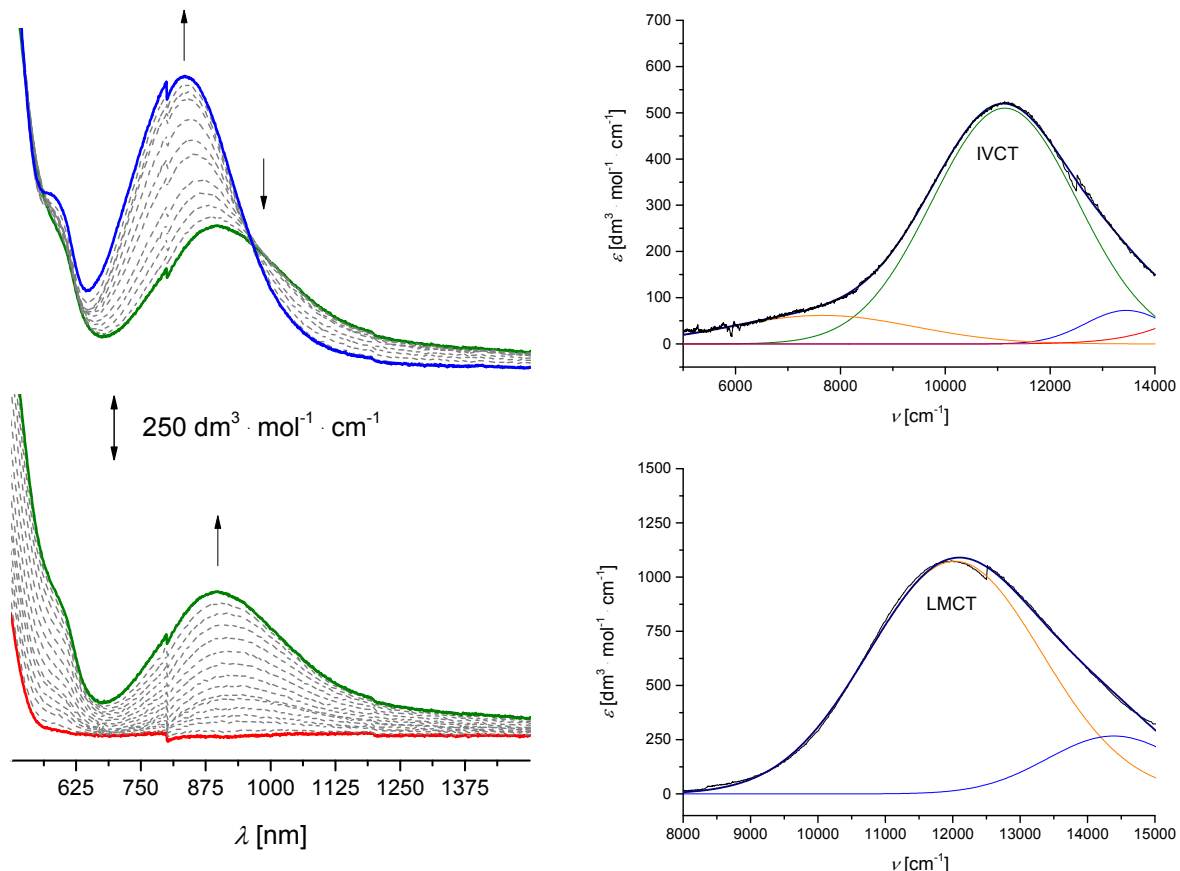


Figure SI37. Left: vis/NIR spectra of 1,5-diferrocenylnaphthalene (**7b**) at 25 °C in dichloromethane (2.00 mmol · L⁻¹) at rising potentials (-200 to 555 mV; top: 555 to 1100 mV vs Ag/Ag⁺); supporting electrolyte [N⁺Bu₄][B(C₆F₅)₄]; arrows indicate the increasing and decreasing absorptions. Right, top: Deconvolution of the NIR absorption of **7b**⁺ using three Gaussian shaped bands. Right, bottom: Deconvolution of NIR absorption of **7b**²⁺ using two Gaussian shaped bands.

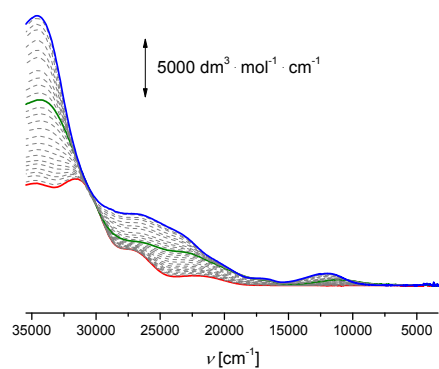


Figure SI38. UV-vis/NIR spectra of 1,5-diferrocenylnaphthalene (**7b**) at 25 °C in dichloromethane (2.00 mmol · L⁻¹) at rising potentials (-200 to 1100 mV vs Ag/Ag⁺); supporting electrolyte [NⁿBu₄][B(C₆F₅)₄].

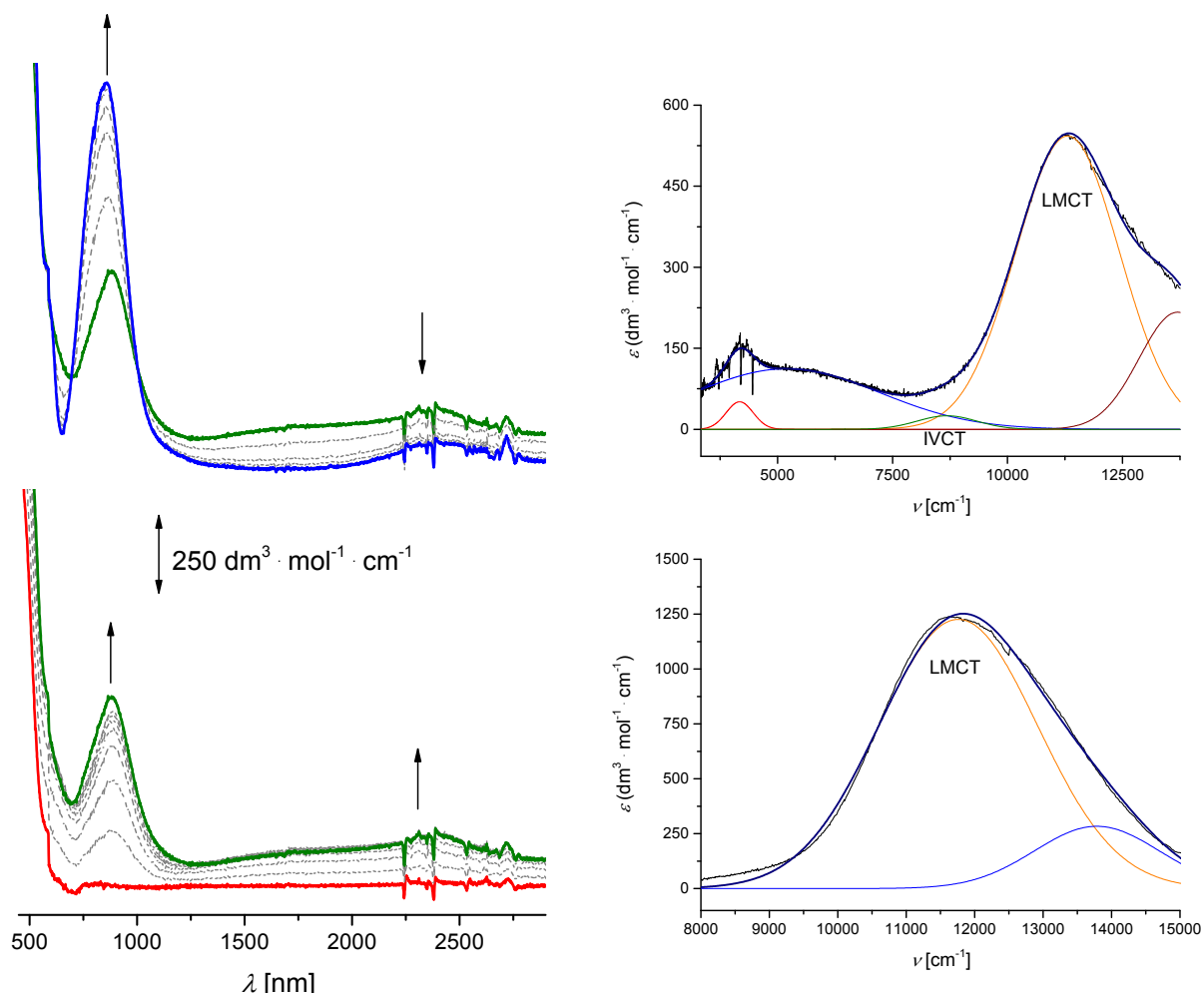


Figure SI39. Left: vis/NIR spectra of 1,8-diferrocenylnaphthalene (**7c**) at 25 °C in dichloromethane (2.00 mmol · L⁻¹) at rising potentials (bottom: -200 to 525 mV; top: 525 to 700 mV vs Ag/Ag⁺); supporting electrolyte [NⁿBu₄][B(C₆F₅)₄]; arrows indicate the increasing and decreasing absorptions. Right, top: Deconvolution of the NIR absorption of **[7c]⁺** using three Gaussian shaped bands. Right, bottom: Deconvolution of NIR absorption of **[7c]²⁺** using two Gaussian shaped bands.

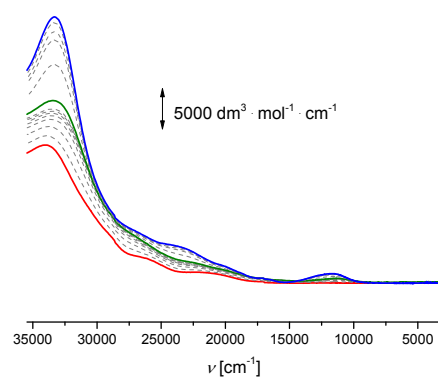


Figure SI40. UV/vis/NIR spectra of 1,8-diferrocenylnaphthalene (**7c**) at 25 °C in dichloromethane (2.00 mmol · L⁻¹) at rising potentials (bottom: -200 to 700 mV vs Ag/Ag⁺); supporting electrolyte [N^tBu₄][B(C₆F₅)₄].

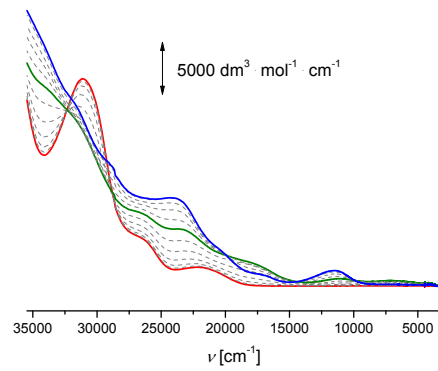


Figure SI41. UV/vis/NIR spectra of 2,6-diferrocenylnaphthalene (**7d**) at 25 °C in dichloromethane (2.00 mmol · L⁻¹) at rising potentials (bottom: -200 to 700 mV vs Ag/Ag⁺); supporting electrolyte [N^tBu₄][B(C₆F₅)₄].

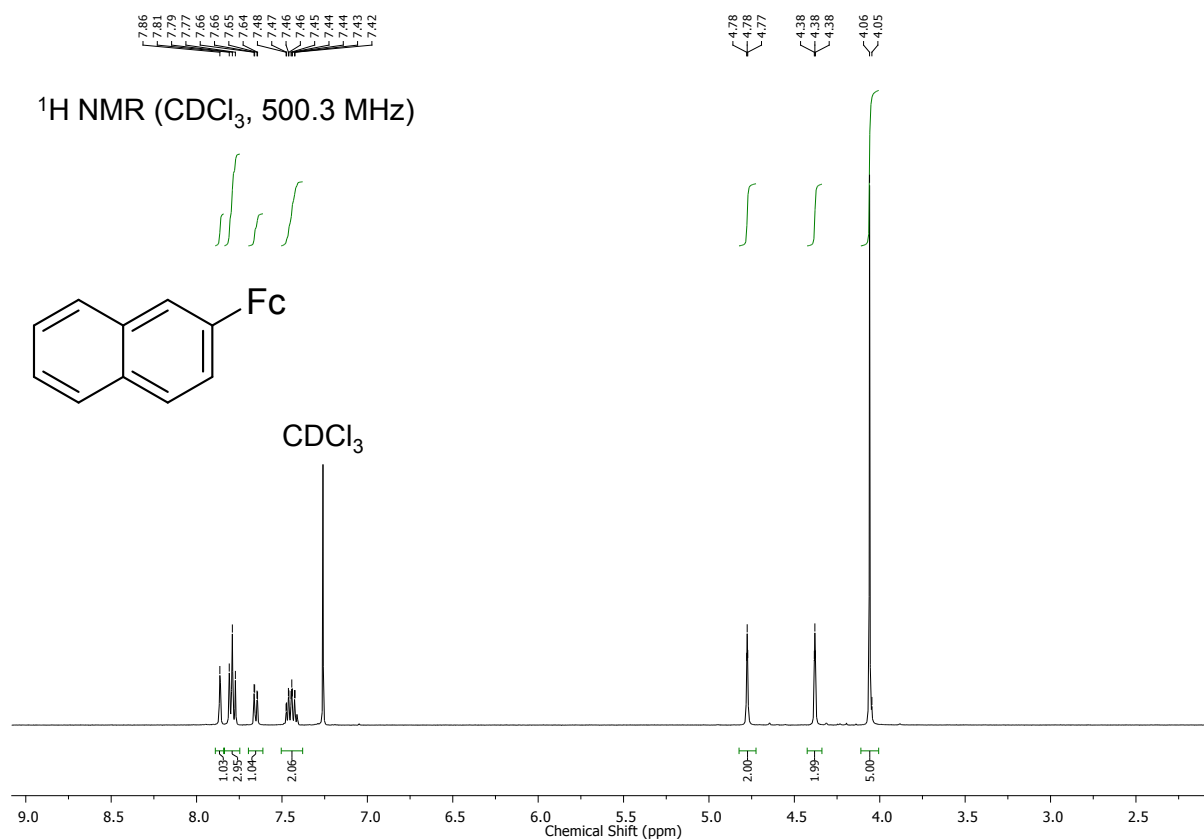


Figure SI42. ¹H NMR spectrum of **3a** in CDCl_3 .

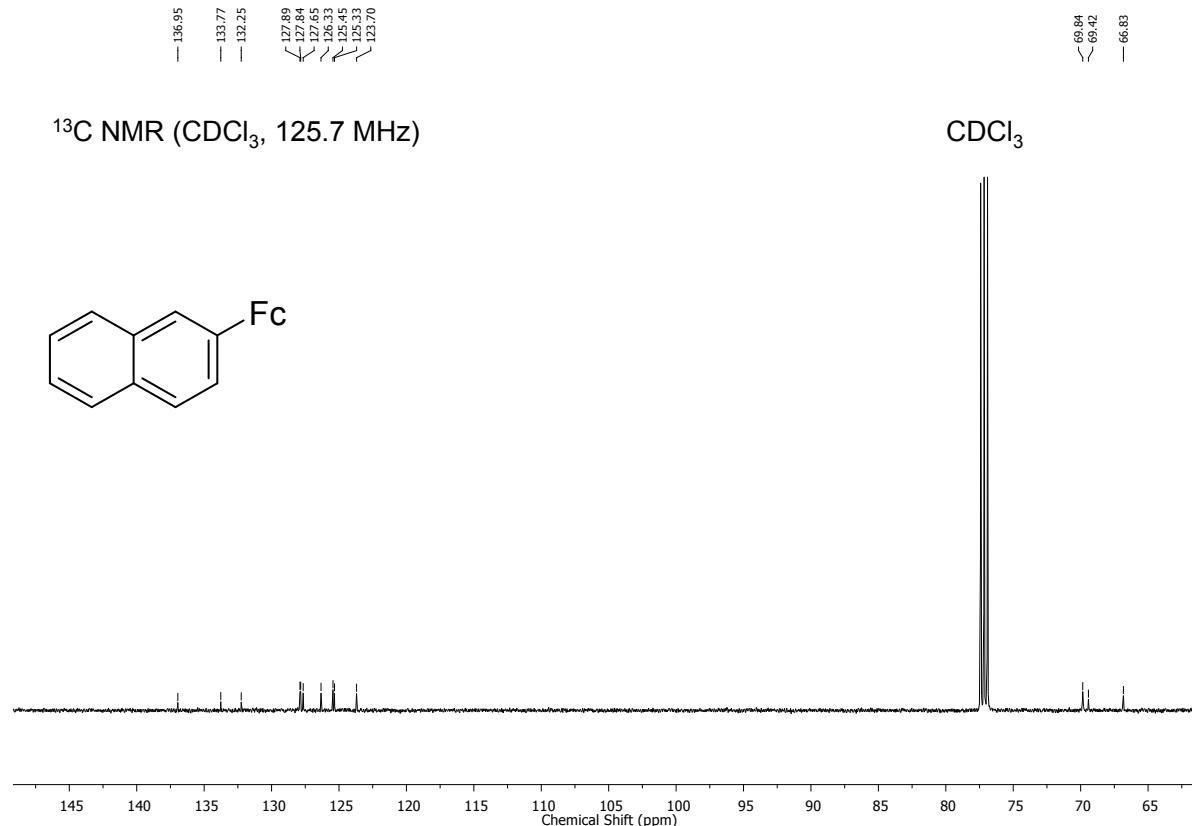


Figure SI43. ¹³C NMR spectrum of **3a** in CDCl_3 .

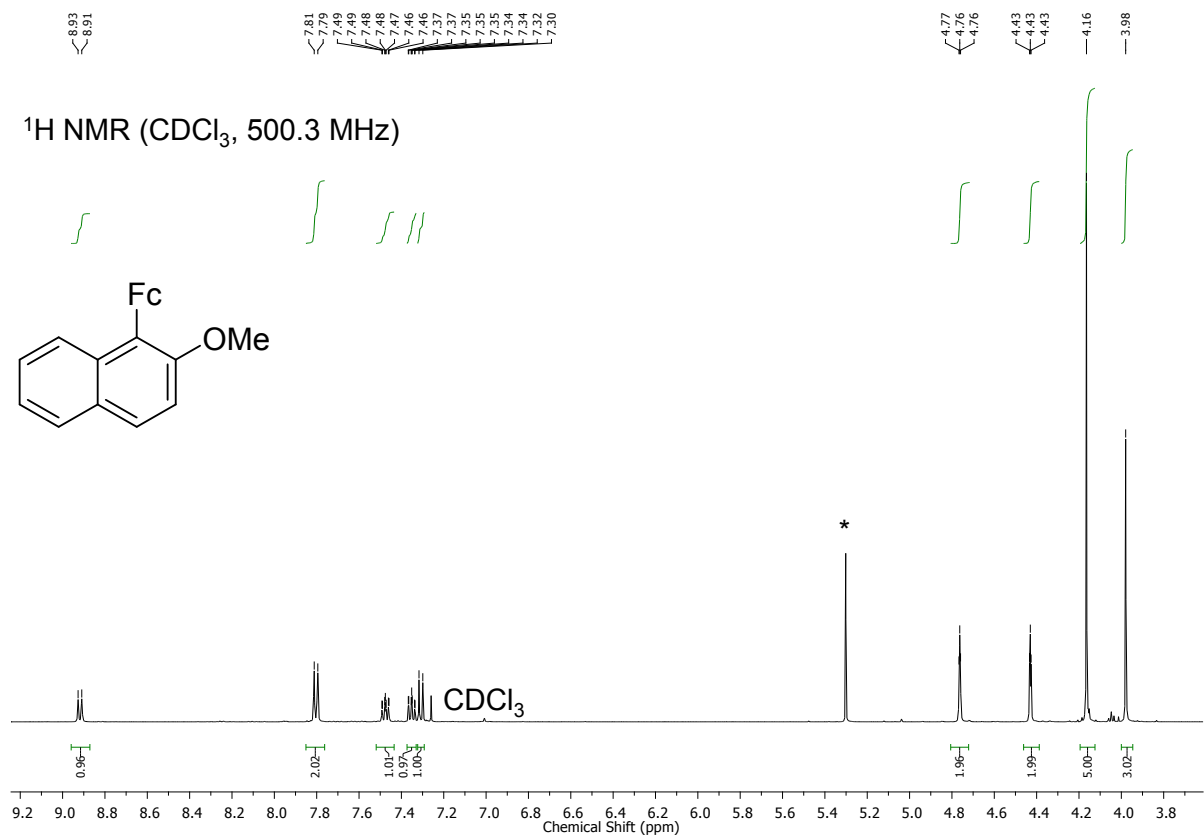


Figure SI44. ¹H NMR spectrum of **3b** in CDCl_3 , * CH_2Cl_2 .

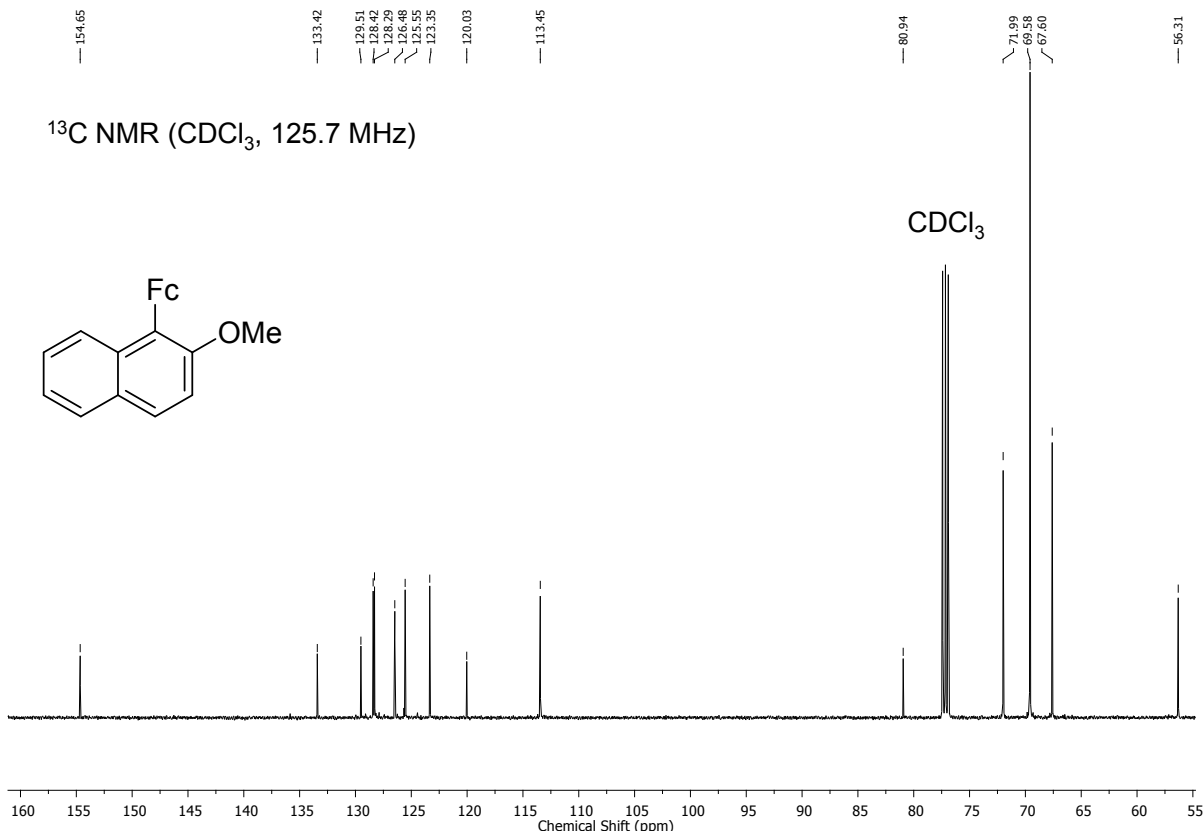


Figure SI45. ¹³C NMR spectrum of **3b** in CDCl_3 .

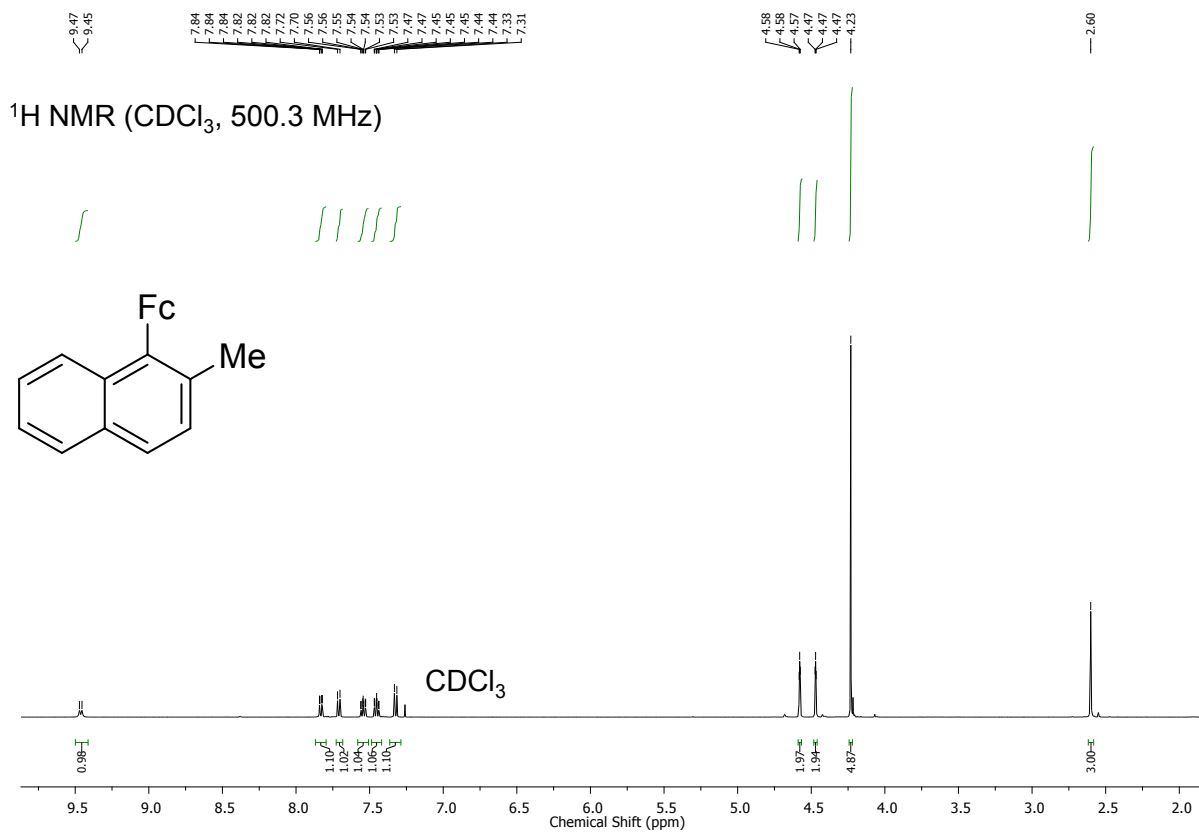


Figure SI46. ¹H NMR spectrum of **3c** in CDCl_3 .

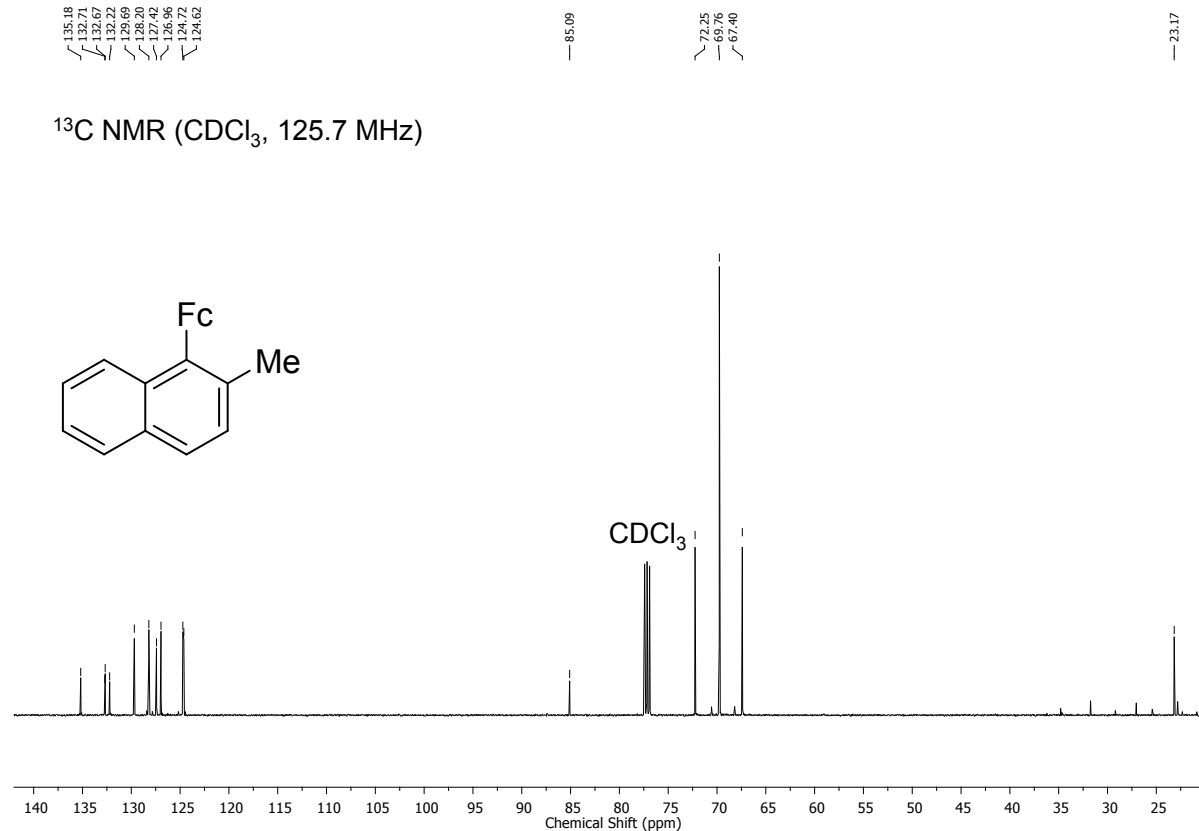


Figure SI47. ¹³C NMR spectrum of **3c** in CDCl_3 .

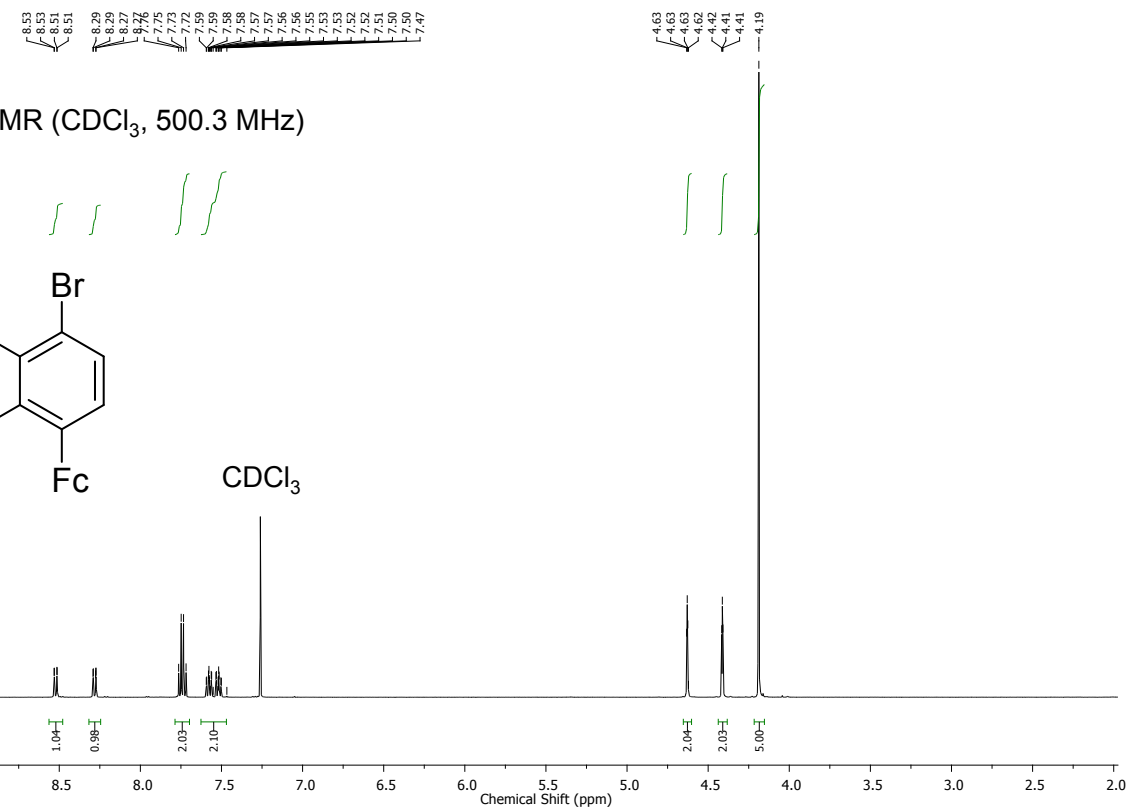


Figure SI48. ¹H NMR spectrum of **6a** in CDCl_3 .

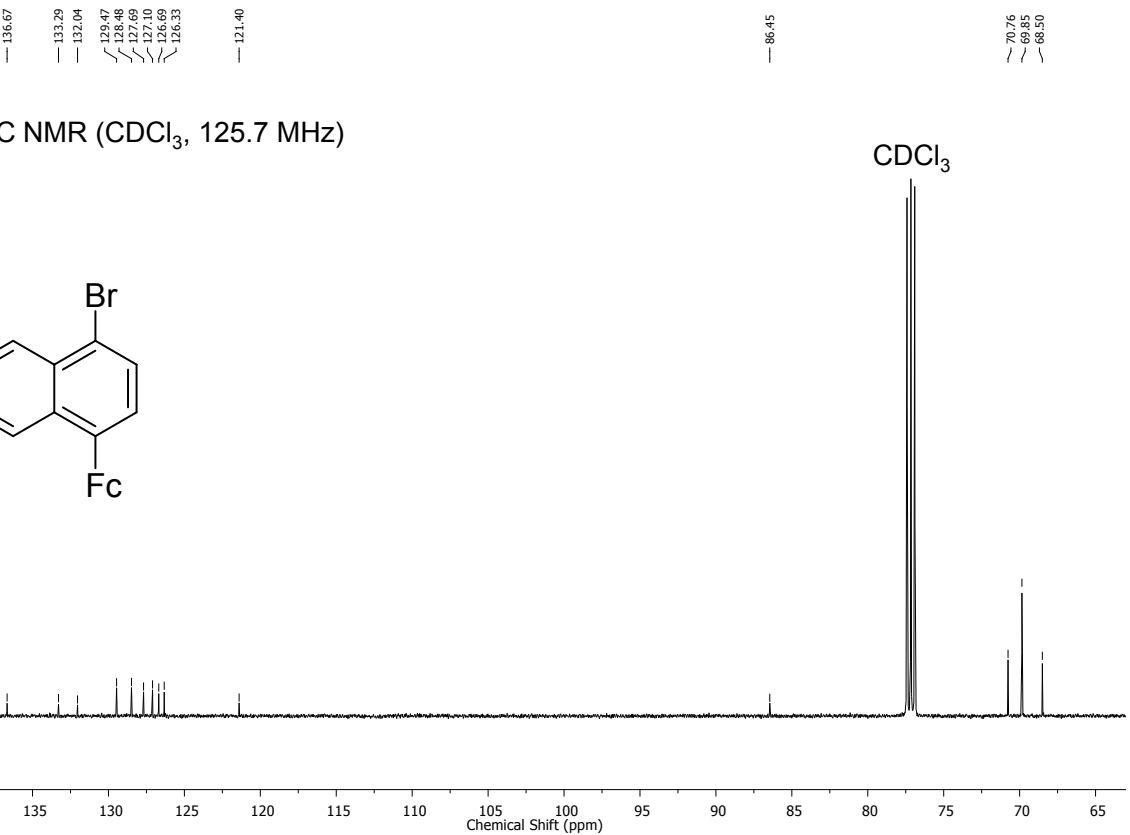


Figure SI49. ¹³C NMR spectrum of **6a** in CDCl_3 .

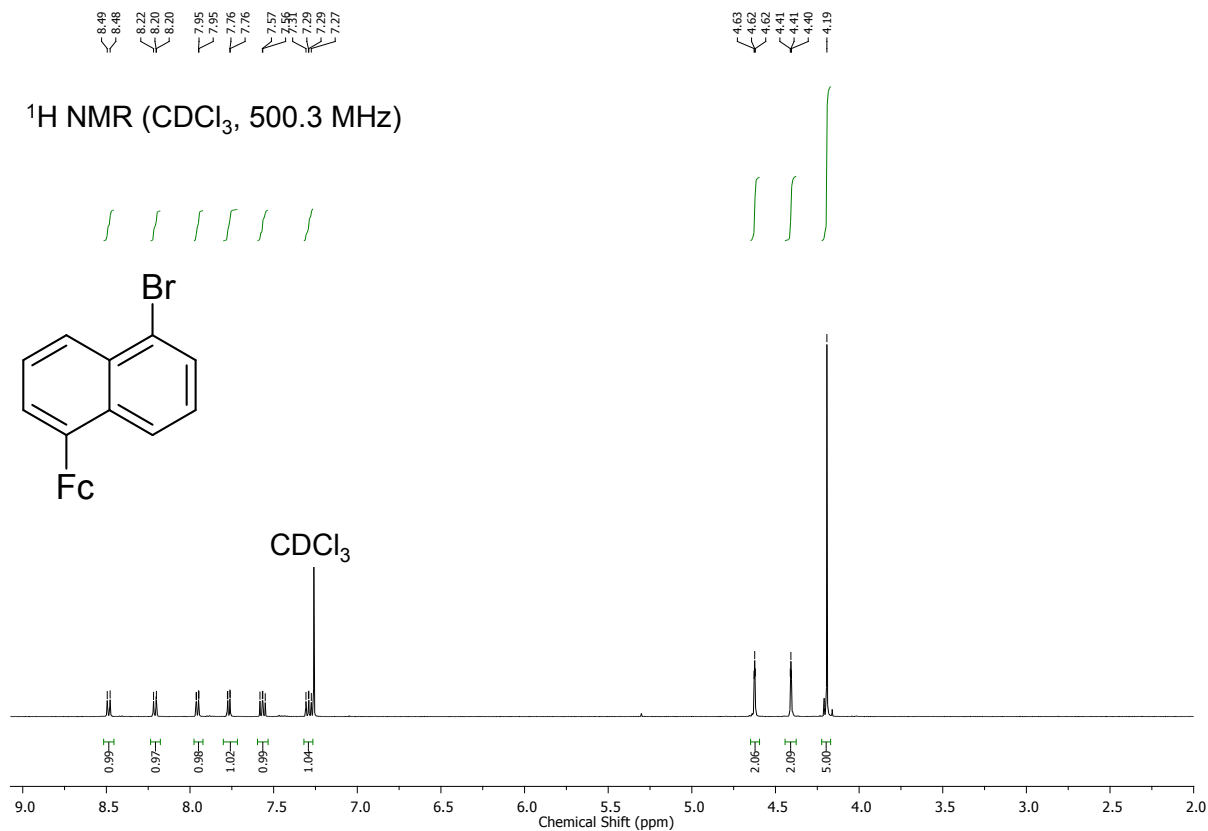


Figure SI50. ^1H NMR spectrum of **6b** in CDCl_3 .

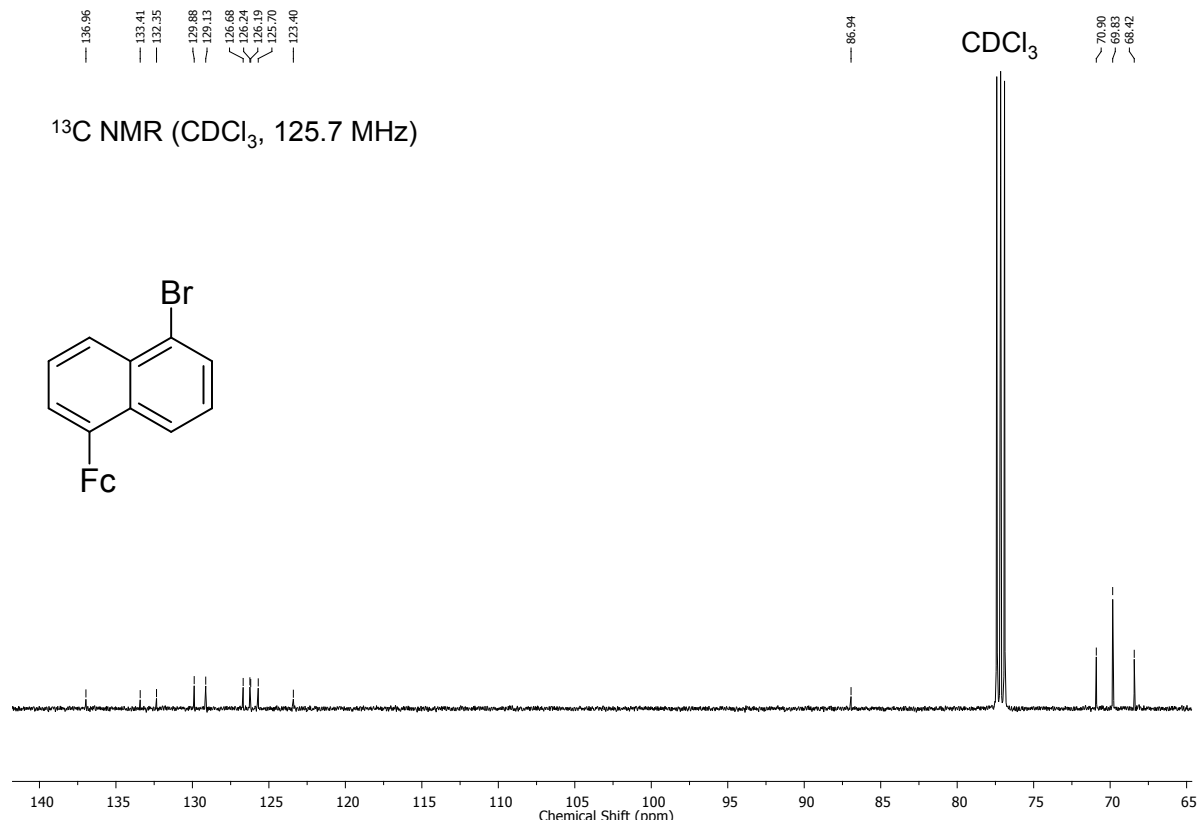


Figure SI51. ^{13}C NMR spectrum of **6b** in CDCl_3 .

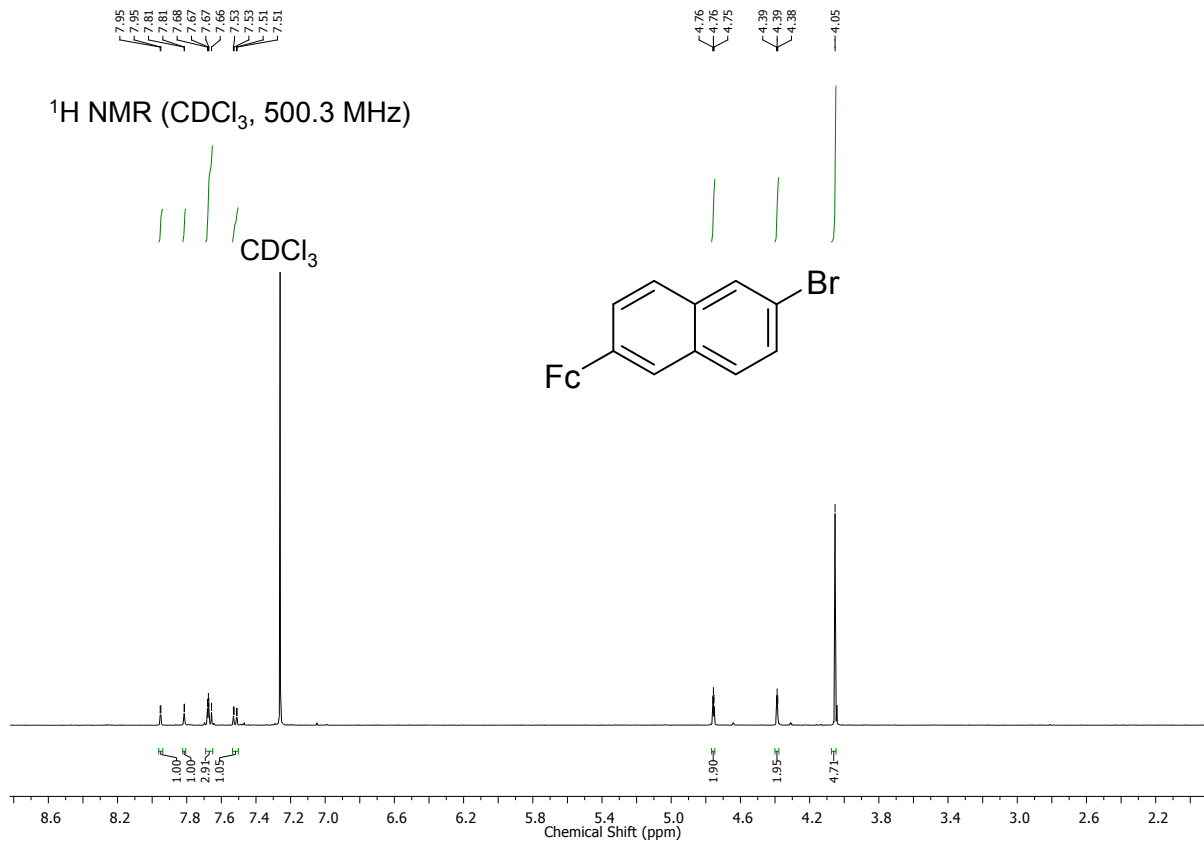


Figure SI52. ¹H NMR spectrum of **6d** in CDCl_3 .

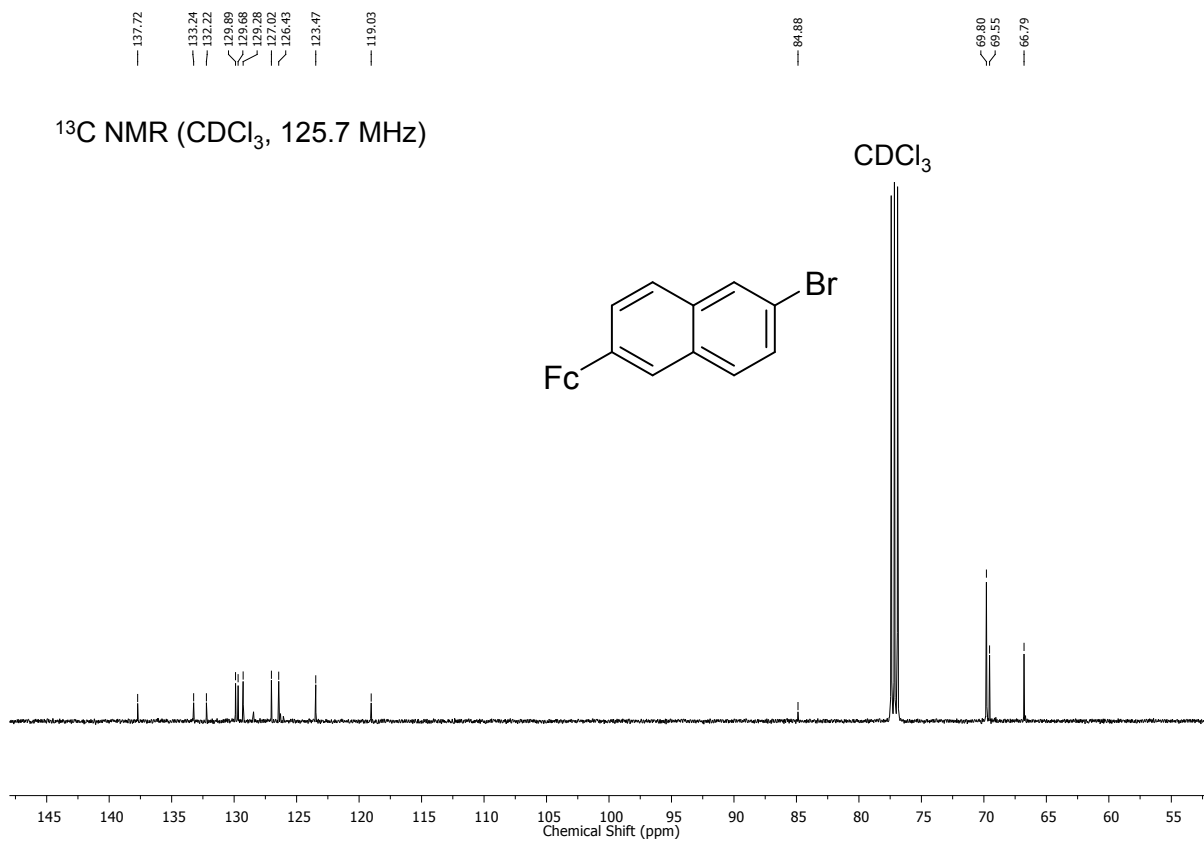


Figure SI53. ¹³C NMR spectrum of **6d** in CDCl_3 .

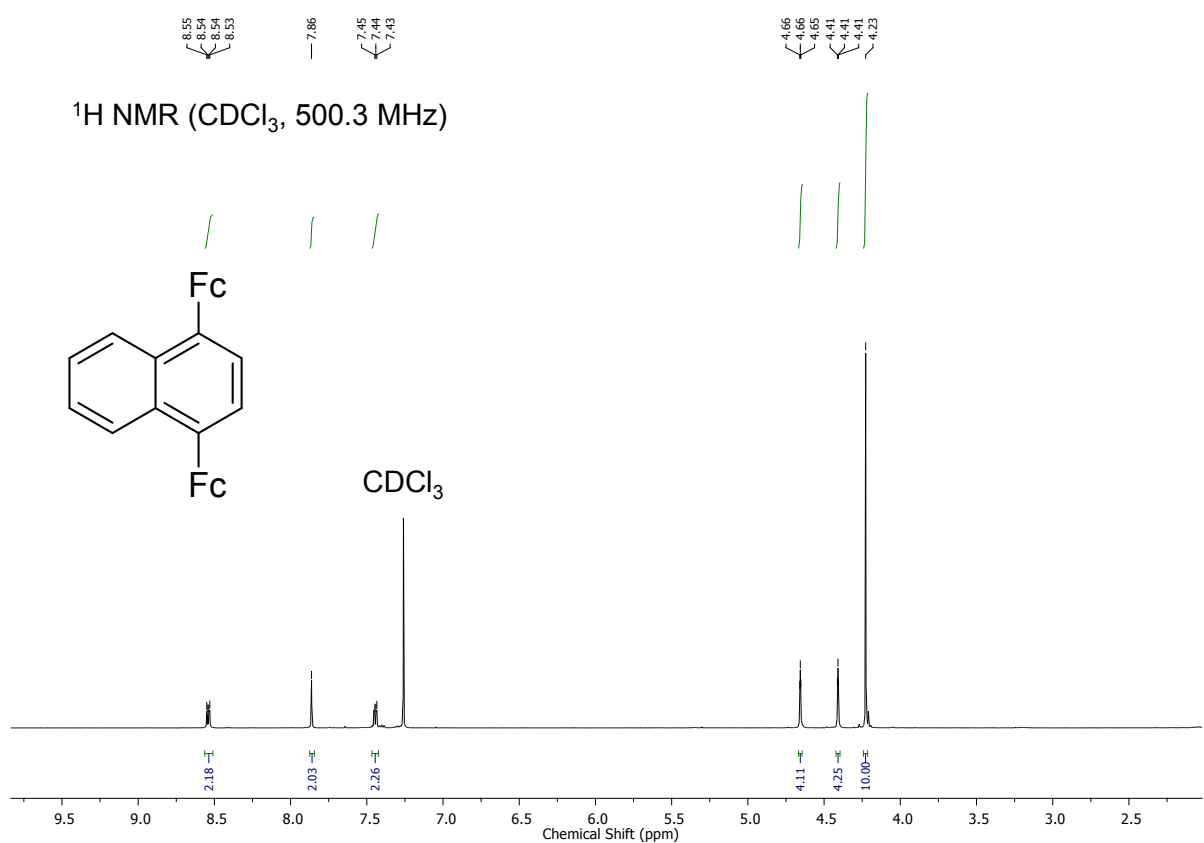


Figure SI54. ¹H NMR spectrum of **7a** in CDCl_3 .

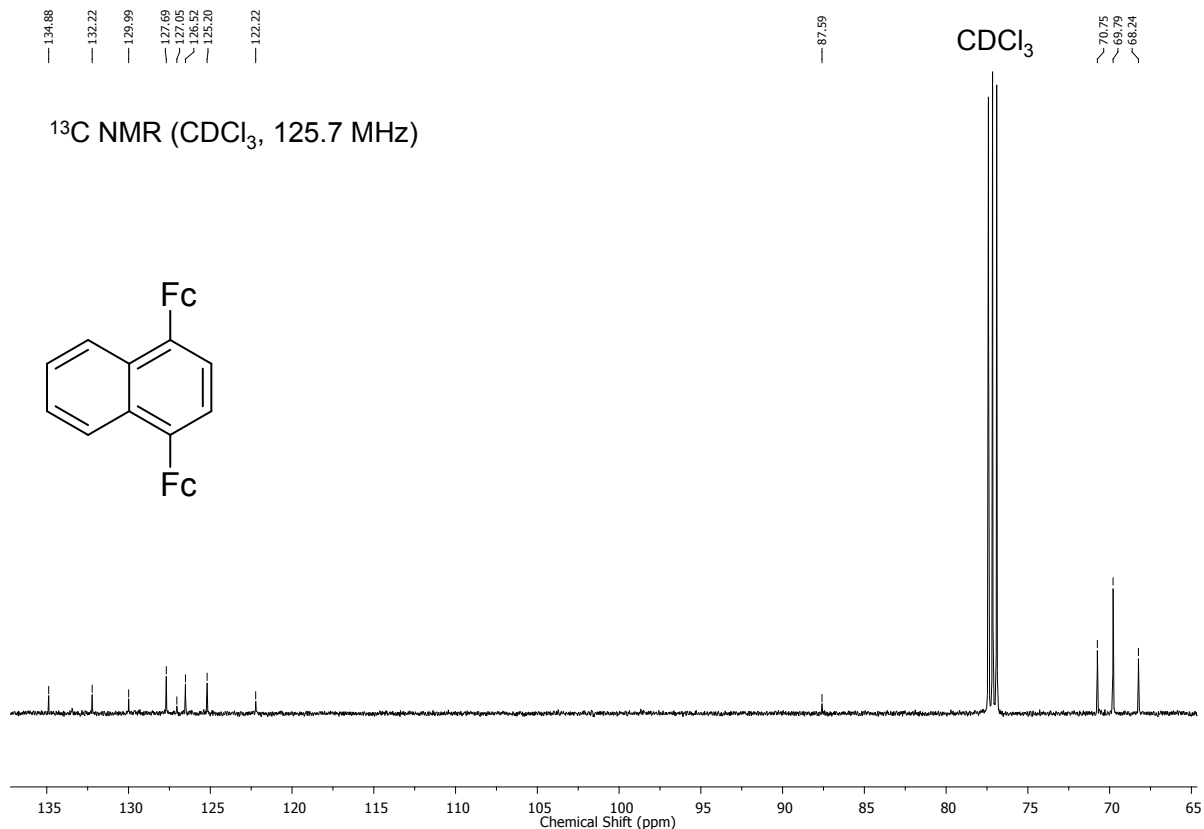


Figure SI55. ¹³C NMR spectrum of **7a** in CDCl_3 .

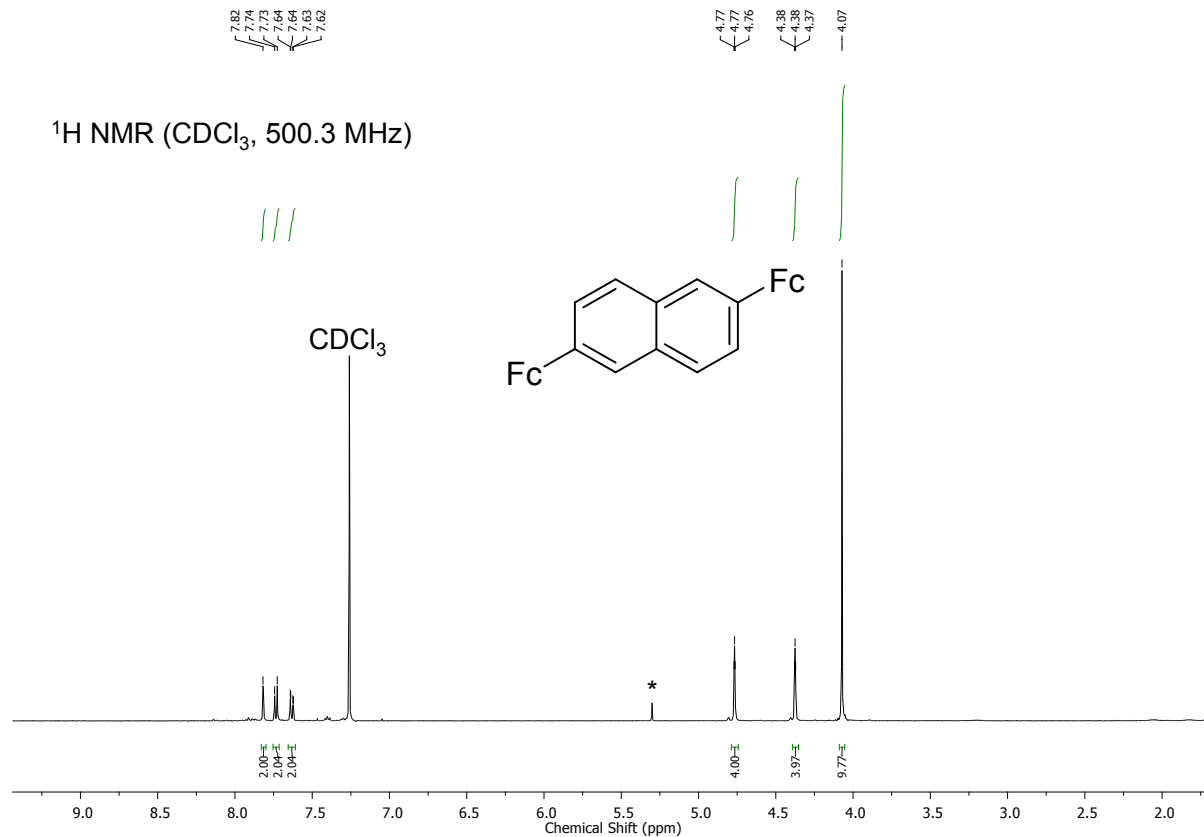


Figure SI56. ¹H NMR spectrum of **7d** in CDCl_3 , $^*\text{CH}_2\text{Cl}_2$.

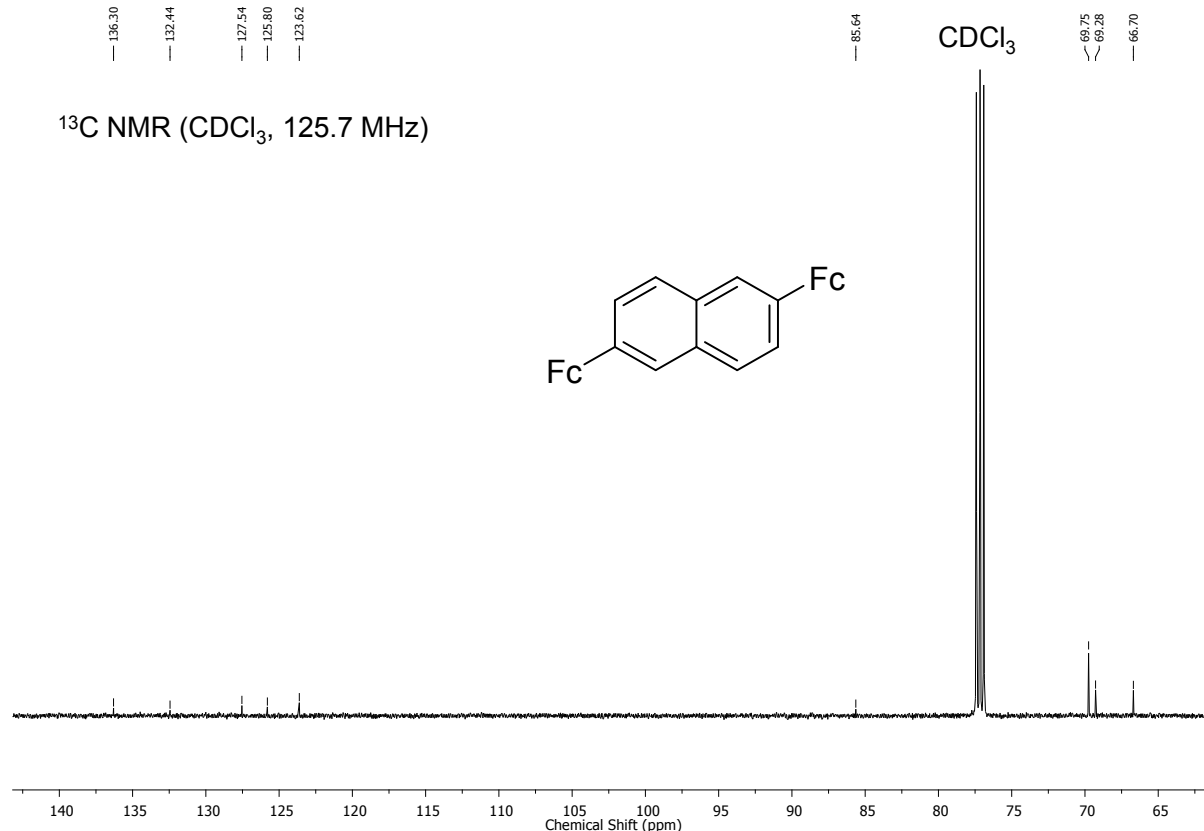


Figure SI57. ¹³C NMR spectrum of **7d** in CDCl_3 .

References

- [1] M. Lee, B. M. Foxman, M. Rosenblum, *Organometallics* **1985**, *4*, 539–547.
- [2] N. Pagels, O. Albrecht, D. Görlitz, A. Y. Rogachev, M. H. Prosenc, J. Heck, *Chem. - A Eur. J.* **2011**, *17*, 4166–4176.
- [3] S. Trtica, M. H. Prosenc, M. Schmidt, J. Heck, O. Albrecht, D. Görlitz, F. Reuter, E. Rentschler, *Inorg. Chem.* **2010**, *49*, 1667–1673.